

Multi-modal contrastive learning adapts to intrinsic dimensions of shared latent variables

Yu Gui¹, Cong Ma¹, and Zongming Ma²

¹Department of Statistics, University of Chicago

²Department of Statistics and Data Science, Yale University

May 20, 2025

Abstract

Multi-modal contrastive learning as a self-supervised representation learning technique has achieved great success in foundation model training, such as CLIP (Radford et al., 2021). In this paper, we study the theoretical properties of the learned representations from multi-modal contrastive learning beyond linear representations and specific data distributions. Our analysis reveals that, enabled by temperature optimization, multi-modal contrastive learning not only maximizes mutual information between modalities but also adapts to intrinsic dimensions of data, which can be much lower than user-specified dimensions for representation vectors. Experiments on both synthetic and real-world datasets demonstrate the ability of contrastive learning to learn low-dimensional and informative representations, bridging theoretical insights and practical performance.

1 Introduction

The growing availability of data sources has enabled interdisciplinary research to leverage *multi-modal* data, which measures each unit from different aspects with various types of information. For example, the availability of data types including images, text, and audio fostered the advancement of cross-modal foundation models in recent years (Li et al., 2019; Lu et al., 2019; Tan and Bansal, 2019; Radford et al., 2021). Another notable example is single-cell multi-omics technologies (Teichmann and Efremova, 2020) which utilize multi-modal measurements of individual cells for more informative scientific discovery (Argelaguet et al., 2020; Kim et al., 2020; Hao et al., 2021; Nandy and Ma, 2024). This emerging phenomenon raises a key question: *How can one efficiently integrate data from multi-modalities?*

Contrastive language-image pre-training (CLIP) was recently proposed in Radford et al. (2021), which utilizes the self-supervised contrastive learning technique to train a vision-language model with unlabeled data and to obtain representations of data from multi-modalities. Mathematically, given observations from two modalities: continuous random vectors $X \in \mathbb{R}^{d_1}$ and $Y \in \mathbb{R}^{d_2}$, the goal of multi-modal contrastive learning is to learn representation maps $f \in \mathcal{H}_X : \mathbb{R}^{d_1} \rightarrow \mathbb{R}^d$ and $g \in \mathcal{H}_Y : \mathbb{R}^{d_2} \rightarrow \mathbb{R}^d$ that map data to representations supported on \mathbb{R}^d , where d is the user-specified output dimension.

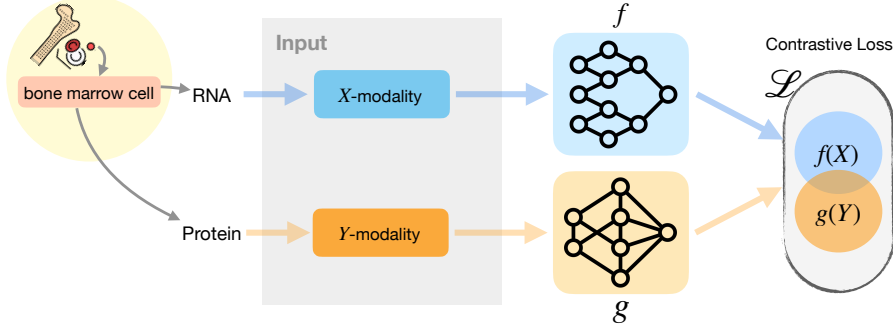


Figure 1: Multi-modal contrastive learning applied to the bone marrow single-cell CITE-seq data.

With a training set $\{(X_i, Y_i)\}_{i \in [N]}$, CLIP Radford et al. (2021) minimizes the infoNCE contrastive loss:

$$\min_{(f, g, \tau) \in \mathcal{H}_X \times \mathcal{H}_Y \times \mathbb{R}_+} \mathcal{L}^N(f, g, \tau) = -\frac{1}{N} \sum_{i \in [N]} \log \frac{\exp\left(\frac{\sigma(f(X_i), g(Y_i))}{\tau}\right)}{N^{-1} \sum_{j \in [N]} \exp\left(\frac{\sigma(f(X_i), g(Y_j))}{\tau}\right)} \quad (1)$$

$$- \frac{1}{N} \sum_{i \in [N]} \log \frac{\exp\left(\frac{\sigma(f(X_i), g(Y_i))}{\tau}\right)}{N^{-1} \sum_{j \in [N]} \exp\left(\frac{\sigma(f(X_j), g(Y_i))}{\tau}\right)},$$

where $\sigma(\cdot, \cdot)$ is a bivariate similarity measure, with larger values of $\sigma(f(X), g(Y))$ indicating higher similarity between embeddings $f(X)$ and $g(Y)$. Here we take into account the optimization over temperature τ to align with the practice of CLIP Radford et al. (2021). In Figure 1, we plot the pipeline of CLIP (Radford et al., 2021) using a bone marrow single-cell CITE-seq dataset (Hao et al., 2021) for illustration.

CLIP has achieved outstanding performance in zero-shot accuracy for downstream tasks and has inspired a number of follow-up works across domains (Galatolo et al., 2021; Li et al., 2021a; Xu et al., 2023; Shi et al., 2023). The theoretical analysis of CLIP was later initialized in Ren and Li (2023), Nakada et al. (2023), and Chen et al. (2023), where the properties of the learned representation and its effect on the downstream accuracy are of interest. However, the distribution of multi-modal data is mainly restricted to factor models with shared latent variables, and the representation map is commonly assumed to be linear, neither of which is close to the actual practice of CLIP. In this paper, we aim to theoretically study the properties of multi-modal contrastive learning with data from general distributions and representation mappings in general function classes.

1.1 A motivating example: CLIP adapts to intrinsic dimension

We begin with describing several interesting phenomena arising from using CLIP on a synthetic data. The phenomena motivate our later theoretic studies.

Consider the synthetic setting where X and Y are generated from the following distribution with $k^* < \min\{d_1, d_2\}$: $Y_i \stackrel{i.i.d.}{\sim} \mathcal{N}(0, \mathbf{I}_{d_2})$, $\xi_i \stackrel{i.i.d.}{\sim} \mathcal{N}(0, \mathbf{I}_{d_1-k^*})$, and $X_i = (Y_{i1}, \dots, Y_{ik^*}, \xi_i^\top)^\top$. We set $k^* = 2$, $d_1 = d_2 = 20$, and the output dimension of $f(X)$ and $g(Y)$ is set to be $d = 3$. We set the function class to be 5-layer ReLU neural networks with all middle-layer widths fixed at 50. We

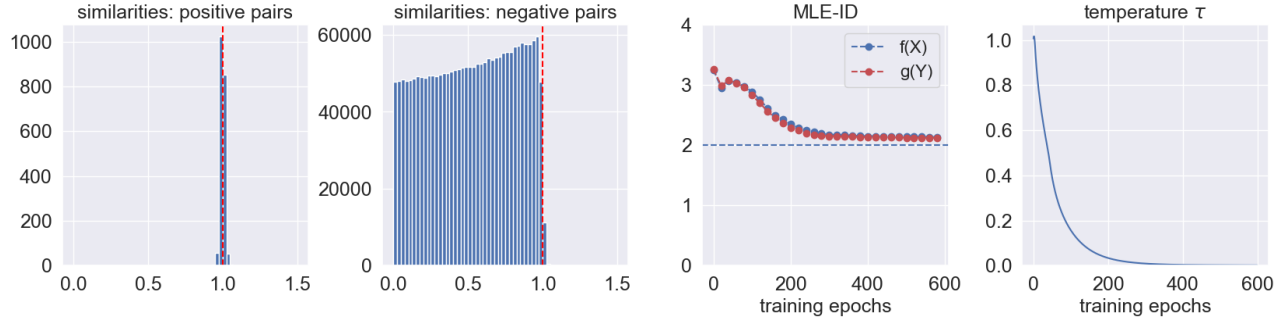


Figure 2: Histograms of out-of-sample similarities, change of intrinsic dimension, and convergence of temperature (linear setting: $k^* = 2$, $d = 3$).

use a training set of size 12000 and a separate test set of size 2000. In the remaining part of this paper, we adopt the inner product with population-level normalization as the similarity measure¹, i.e., $\sigma(f(X), g(\tilde{Y})) = \frac{\langle f(X), g(\tilde{Y}) \rangle}{\mathbb{E}\|f(X)\| \cdot \mathbb{E}\|g(\tilde{Y})\|}$. In experiments, we leave out a fixed subset of size 2000 of the training set to estimate expected norms in each iteration. In Figure 2, we plot the *out-of-sample* similarities between positive and negative pairs, the change of estimated intrinsic dimension along training (see Section 4 for further details), and temperature τ along training. We note the following phenomena from the results:

1. For positive pairs, $\sigma(f(X_i), g(Y_i))$ tends to concentrate around one, while similarities between negative pairs are capped by one;
2. Although the output dimension is 3, representations with intrinsic dimension 2 instead of 3 are preferred by infoNCE loss;
3. The optimized temperature converges to *zero*.

The observed phenomena, especially the intrinsic dimension selection and the convergence of temperature to zero, motivate us to understand multi-modal contrastive learning via CLIP from the theoretical perspective in this work.

1.2 Why existing understanding of multi-modal contrastive learning is insufficient?

Existing work explains the representations learned by contrastive learning from two different perspectives. Here, we elaborate on why neither can fully explain the phenomena observed in Section 1.1.

Perspective from alignment and uniformity Wang and Isola (2020) decomposes the population infoNCE loss \mathcal{L} into alignment and uniformity terms such that $\mathcal{L}(f, g, \tau) = \mathcal{L}_{\text{align}}(f, g, \tau) + \mathcal{L}_{\text{unif}}(f, g, \tau)$. The first term $\mathcal{L}_{\text{align}}$ favors alignment as it is minimized when $f(X) = g(Y)$ almost surely. In addition, the result in Wang and Isola (2020) implies that among all aligned representations, the second term $\mathcal{L}_{\text{unif}}$ favors uniformity as it is minimized when $f(X)$ is uniformly distributed over the entire output

¹In Appendix G.5, we show that it is comparable to cosine similarity in terms of both representation intrinsic dimensions and downstream task performances.

space, which is restricted to be the unit hypersphere with a *user-specified dimension* in Wang and Isola (2020). A crucial limitation of this result is that one needs the correct specification of a *true dimension* of data. In other words, if the aligned representation has a smaller dimension compared to the ambient output dimension (which arguably is always the case in practice) or the function class is not expressive enough to produce uniform representations on the entire output space, the theory established in Wang and Isola (2020) is not applicable.

Perspective from mutual information maximization Since the infoNCE loss can be viewed as a variational upper bound of the negative mutual information (Oord et al., 2018; Poole et al., 2019) (see also Lemma 8 below), another line of research understands the global minimizer of infoNCE loss as the mutual information maximizer (Uesaka et al., 2024; Hjelm et al., 2018; Tschannen et al., 2019; Tian et al., 2020; Zimmermann et al., 2021; Li et al., 2021b). Although existing works connect infoNCE loss to its mutual information bound, as is pointed out in Tschannen et al. (2019), solely maximizing the mutual information may result in undesirable representations. For instance, in the example in Section 1.1, as long as $f(X) \approx g(Y)$ almost surely,² the mutual information between representations is infinite. Hence, this theory fails to explain why, in the motivating example, $f(X)$ and $g(Y)$ are supported on a 2-dimensional manifold as opposed to a curve or a number of standalone points, since the latter two can also maximize mutual information between representations at infinity. This indicates that infoNCE loss minimization is not simply mutual information maximization and requires a more fine-grained analysis.

1.3 Preview of our results and contributions

We now provide a preview of our main theoretical findings that allow us to explain the three phenomena observed in Section 1.1. A formal version will be presented in Section 3.

Theorem 1 (Informal). *Suppose there exist aligned representations that maximize the shared information between X and Y . Then, any “minimizer” (f, g, τ) of the infoNCE loss satisfies*

1. $\sigma(f(X), g(Y)) = \text{constant almost surely, which caps similarities between negative pairs;}$
2. $\text{the intrinsic dimension of shared latent variables in the multi-modal data is exactly captured by } (f(X), g(Y)).$
3. $\tau = 0^+.$

In addition, we summarize our contributions in this paper as follows.

- We investigate the theoretical properties of *learned representations* from multi-modal contrastive learning and take into account *temperature optimization* in theoretical analysis.
- Based on a precise (variational) decomposition of the infoNCE loss in Lemma 8, we theoretically show that temperature optimization enables multi-modal contrastive learning, which encourages multi-modal representations to be sufficient and to maximize the similarity measure, to also

²Throughout this paper, “almost surely” refers to almost sure events with respect to the joint distribution of (X, Y) , unless otherwise specified. Likewise, “measurable” refers to measurability with respect to the Lebesgue measure, unless stated otherwise.

adapt to the intrinsic dimension of data. To be more concrete, different from Wang and Isola (2020), our theory does not require the existence of aligned representations that are uniform over the entire output space, i.e., no prior knowledge about the true intrinsic dimension is required.

- Moreover, the practical relevance of our theory is supported by empirical findings in real-world datasets, such as single-cell multi-omics and image-text datasets, which demonstrate that in many cases, there are a relatively small number of effective shared features that affect downstream tasks.

Organization of paper. The rest of this paper is organized as follows. The ideal properties of representations and the intrinsic dimension are formally defined in Section 2. Main theoretical results are shown in Section 3, which includes a formal statement of our theorem in Section 3.2. Additional related works are summarized in Section 5. Experimental results for both synthetic and CITE-seq single-cell datasets are presented in Section 4. Technical proofs, extensions (e.g., connection to sufficient dimension reduction in Appendix E.1), and additional numerical experiments are deferred to the appendix.

2 Ideal representations and intrinsic dimension

In Section 2.1, we define two key properties of the ideal representations $(f^*(X), g^*(Y))$ when learning from the paired data (X, Y) —alignment and maximal mutual information, and in Section 2.2, we define the intrinsic dimension. Throughout the paper, we define $\mathcal{H} = \mathcal{H}_X \times \mathcal{H}_Y$.

2.1 Alignment and maximal mutual information

Alignment and similarity maximization. Inspired by the seminal work (Wang and Isola, 2020) in single-modality contrastive learning, we propose the following notion of *alignment* for learning representations from multiple modalities.

Definition 1. We define the set of representation maps that realize alignment and similarity maximization as

$$\mathcal{A}(\mathcal{H}) = \left\{ (f, g) \in \mathcal{H} : \frac{f(X)}{\mathbb{E}\|f(X)\|} = \frac{g(Y)}{\mathbb{E}\|g(Y)\|}, \quad \sigma(f(X), g(Y)) = m_\sigma(f, g) \text{ almost surely} \right\}.$$

Here and after, $m_\sigma(f, g) := \text{ess sup}_{X \perp\!\!\!\perp \tilde{Y}} \sigma(f(X), g(\tilde{Y}))$ for any $(f, g) \in \mathcal{H}$.

In our motivating example in Section 1.1, there exist representations $f(X) = (X_1, X_2)/\sqrt{X_1^2 + X_2^2} = (Y_1, Y_2)/\sqrt{Y_1^2 + Y_2^2} = g(Y)$ satisfying $(f, g) \in \mathcal{A}(\mathcal{H})$. In this case, $\sigma(f(X), g(Y)) = 1 = m_\sigma(f, g)$ almost surely.

Maximal mutual information. A classical notion to measure statistical dependence is mutual information: $I(X; Y) = D_{\text{KL}}(P_{X,Y} \parallel P_X \otimes P_Y)$. It is tempting to ask for representations (f, g) such that the mutual information $I(f(X); g(Y))$ is maximized. This is known as the infoMax principle (Tschannen et al., 2019; Bachman et al., 2019). However, as we have argued in Section 1.2, this

vanilla definition of mutual information is not fine-grained enough to compare aligned representations: whenever continuous representations $f(X) = g(Y)$ almost surely, we have $I(f(X); g(Y)) = +\infty$ (Laughlin, 1981; Tishby and Zaslavsky, 2015).

To mitigate the deficiency, we adopt a fine-grained *order* for mutual information. For each integer $M \geq 1$, we consider a discretized version³ (f_M, g_M) of the representations (f, g) . As (f_M, g_M) are supported on finitely many points, the mutual information $I(f_M(X); g_M(Y))$ is always finite, albeit $\lim_{M \rightarrow +\infty} I(f_M(X); g_M(Y))$ is possibly infinite.

With the discretization in place, we can define the set of representations with maximal mutual information as follows.

Definition 2 (Maximal mutual information). We define the following set of pairs $(f, g) \in \mathcal{H}$ that sufficiently capture the dependence between X and Y :

$$\mathcal{W}(\mathcal{H}) = \{(f, g) \in \mathcal{H} : \liminf_{M \rightarrow +\infty} (I(f_M(X); g_M(Y)) - I_M^*(\mathcal{H})) \geq 0\},$$

where $I_M^*(\mathcal{H}) = \sup_{(f, g) \in \mathcal{H}} I(f_M(X); g_M(Y))$.

Roughly speaking, representations (f, g) have maximal mutual information if at every discretization level M , the mutual information $I(f_M(X); g_M(Y))$ is comparable to the maximal discrete mutual information $I_M^*(\mathcal{H})$ achievable by the function class. In our motivating example in Section 1.1, where the shared latent variables between X and Y are two-dimensional, the learned representations can maximize mutual information only if they can capture all the latent features and have the intrinsic dimension of 2.

In the end, we define $\mathcal{V}(\mathcal{H}) = \mathcal{A}(\mathcal{H}) \cap \mathcal{W}(\mathcal{H})$. Throughout the paper, we assume $\mathcal{V}(\mathcal{H}) \neq \emptyset$, i.e., there exist aligned representations with maximal mutual information.

2.2 Intrinsic dimension

We now move on to define the intrinsic dimension of a representation function f . To begin with, we define the range of a function f to be $R(f) = \{f(x) : x \in \mathbb{R}^{d_1}\}$, and define the usual linear dimension as $\dim(R(f)) = \dim(\text{span}(R(f)))$. However, this vanilla dimension is not able to capture the nonlinearity in f , and the possible manifold structure in the range of f . With this in mind, we adopt the following notion of intrinsic dimension, which is closely related to the dimension of manifolds (Lee and Lee, 2003).

Definition 3 (Intrinsic dimension.). We define the intrinsic dimension of $f \in \mathcal{H}_X$, denoted by $\text{ID}(f)$, as the smallest integer k such that there exist a measurable function $h : \mathbb{R}^{d_1} \rightarrow \mathbb{R}^d$ with $\dim(R(h)) = k$ and an injective measurable function $\phi : R(h) \rightarrow \mathbb{R}^d$ such that $f(x) = (\phi \circ h)(x)$ almost everywhere.

As an example, with a full-rank matrix $\mathbf{A} \in \mathbb{R}^{k \times d_Z}$ and an injective map $\zeta : \mathbb{R}^k \rightarrow \mathbb{R}^d$, the representation $f(Z) = \zeta(\mathbf{A}Z)$, which is usually known as the multi-index model (Xia, 2008; Li, 1991), has intrinsic dimension exactly k where we can choose $h(Z) = \mathbf{A}Z$ and $\phi = \zeta$.

³See Section A.2 for precise definitions of the discretizations. Related results on approximating mutual information based on discretization and binning can also be found in Kraskov et al. (2004); Paninski (2003); Cover (1999).

Proposition 1. *Suppose $\mathcal{V}(\mathcal{H}) \neq \emptyset$. Then all ideal representations $(f, g) \in \mathcal{V}(\mathcal{H})$ have the same intrinsic dimension k^* , that is, for all $(f, g) \in \mathcal{V}(\mathcal{H})$, we have $\text{ID}(f) = \text{ID}(g) = k^*$.*

To further understand the definition of k^* , we recall the example in Section 1.1. As the shared feature between X and Y has dimension 2, any aligned representations supported on a curve cannot maximize the mutual information with a certain function class. Also, any representations with intrinsic dimension larger than 2 will have additional randomness conditioning on the 2-dimensional shared feature, and thus cannot align.

3 Global minimizers of InfoNCE and dimension adaptation

In this section, we analyze the global minimizers of the population infoNCE loss and prove that CLIP adapts to the intrinsic dimension k^* of the ideal representations.

3.1 InfoNCE loss and its minimizers

Similar to prior work (Wang and Isola, 2020; Liu et al., 2024), throughout the paper, we consider the population infoNCE loss

$$\mathcal{L}(f, g, \tau) = -\mathbb{E}_{X,Y} \left[\log \frac{\exp\left(\frac{\sigma(f(X), g(Y))}{\tau}\right)}{\mathbb{E}_{\tilde{Y}} \exp\left(\frac{\sigma(f(X), g(\tilde{Y}))}{\tau}\right)} \right] - \mathbb{E}_{X,Y} \left[\log \frac{\exp\left(\frac{\sigma(f(X), g(Y))}{\tau}\right)}{\mathbb{E}_{\tilde{X}} \exp\left(\frac{\sigma(f(\tilde{X}), g(Y))}{\tau}\right)} \right], \quad (2)$$

where $\tilde{Y} \stackrel{d}{=} Y$, $\tilde{X} \stackrel{d}{=} X$, and $(\tilde{X}, \tilde{Y}) \perp\!\!\!\perp (X, Y)$. Based on Wang and Isola (2020) (Theorem 1) and Liu et al. (2024) (Theorem 2.1), the population loss (2) is indeed the large-sample limit of the empirical loss (1) as $\lim_{N \rightarrow +\infty} |\mathcal{L}^N(f, g, \tau) - \mathcal{L}(f, g, \tau)| = 0$, for any fixed f, g , and $\tau > 0$.

Temperature optimization. We consider the regime where the temperature $\tau \geq 0$ is also optimized in the training process, which aligns with the practice (Radford et al., 2021). In previous theoretical works on CLIP, the temperature parameter was either treated as fixed (Wang and Isola, 2020) or not taken into account (Nakada et al., 2023; HaoChen et al., 2021). However, it has been revealed in both empirical and theoretical studies that different choices of τ can lead to extremely different properties of the learned representations (Wang and Isola, 2020; Wang and Liu, 2021; Geiping et al., 2023; Gui et al., 2023). Thus, to theoretically understand properties of representations learned by CLIP in practice, we take temperature optimization into account and write τ as an argument of the loss function.

Minimizers of the infoNCE loss. Challenges arise when defining the tuple (f, g, τ) that minimizes the infoNCE loss in (2). Consider two representations (f_1, g_1) and (f_2, g_2) . Both are aligned and continuous. It can be shown that $\lim_{\tau \rightarrow 0^+} \mathcal{L}(f_1, g_1, \tau) = -\infty = \lim_{\tau \rightarrow 0^+} \mathcal{L}(f_2, g_2, \tau)$. In other words, the infoNCE loss cannot differentiate among aligned continuous representations, due to the unboundedness of mutual information for aligned continuous representations.

To address this issue, we use the same discretization idea in Section 2.1. Precisely, for each slackness $\eta > 0$, we define the set of near-minimizers to be

$$\mathcal{O}_{\mathcal{L},\eta}(\mathcal{H}) = \left\{ (f, g) \in \mathcal{H} : \exists \tau \geq \varepsilon(\eta), \limsup_{M \rightarrow +\infty} (\mathcal{L}(f_M, g_M, \tau) + 2I_M^*(\mathcal{H})) \leq 2\eta \right\}, \quad (3)$$

where $\varepsilon(\eta) > 0$ is nondecreasing⁴ in η with $\varepsilon(0) = 0$. Correspondingly, we define the set of minimizers to be $\bigcap_{\eta \geq 0} \mathcal{O}_{\mathcal{L},\eta}(\mathcal{H})$. A few remarks are in order.

- First, instead of looking at $\mathcal{L}(f, g, \tau)$ which could be $-\infty$, we compare its discretized version $\mathcal{L}(f_M, g_M, \tau)$ against a benchmark $-2I_M^*(\mathcal{H})$. Both quantities are finite.
- Second, the lower bound $\varepsilon(\eta)$ on the temperature measures the sensitivity of the solution (f, g) with respect to the change of temperature τ . Then, with any tolerance $\eta > 0$, the set $\mathcal{O}_{\mathcal{L},\eta}(\mathcal{H})$ only contains representation maps that achieve small loss with temperature no less than the threshold $\varepsilon(\eta)$ and hence rules out the representations that can only be optimal in the singular case when the temperature is always zero, which is in line with the fact that the temperature can only decrease to zero at a certain rate in the actual training process.

3.2 CLIP automatically adapts to intrinsic dimensions

Recall the definition of k^* in Proposition 1. We now present the main result, assuming that \mathcal{H} includes all measurable functions of X and Y .

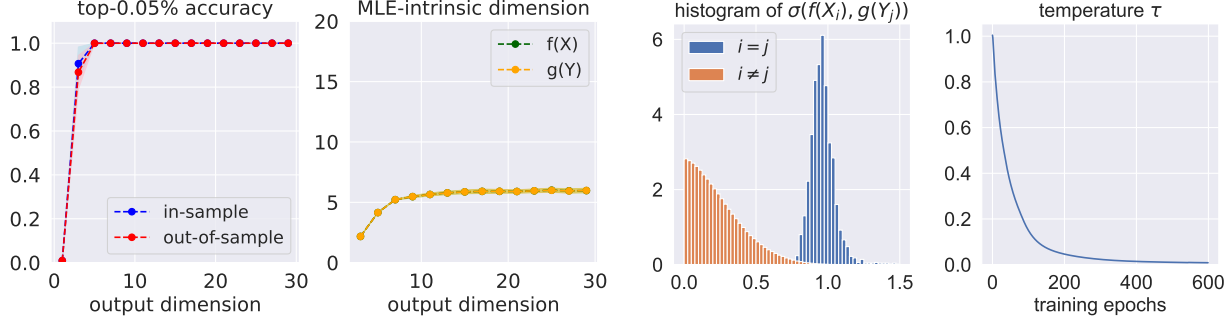
Theorem 2. *Assume that $\mathcal{V}(\mathcal{H}) \neq \emptyset$. We have $\bigcap_{\eta \geq 0} \mathcal{O}_{\mathcal{L},\eta}(\mathcal{H}) \neq \emptyset$. In addition, for any $(f, g) \in \bigcap_{\eta \geq 0} \mathcal{O}_{\mathcal{L},\eta}(\mathcal{H})$, we have*

1. (*similarity maximization*) $\sigma(f(X), g(Y)) = m_\sigma(f, g)$ almost surely;
2. (*intrinsic dimension adaptation*) $\text{ID}(f) = \text{ID}(g) = k^*$;
3. (*monotonicity in temperature*) infoNCE loss $\mathcal{L}(f, g, \tau)$ is increasing in τ ;
4. (*mutual information maximization*) $(f, g) \in \mathcal{W}(\mathcal{H})$.

Theorem 2 implies that (approximate) minimizers of the InfoNCE loss have an intrinsic dimension exactly equal to k^* . We note that the existence of aligned and uniformly distributed representations over the entire output space, as required in Wang and Isola (2020), provides a sufficient condition for $\mathcal{V}(\mathcal{H}) \neq \emptyset$. In contrast, our result shows that even without requiring representations to be aligned and uniform over the entire output space, CLIP can still adapt to the intrinsic dimension of multi-modal data. As a corollary, in Appendix E.2, we further show that when the output dimension d is correctly specified, the set of minimizers $\bigcap_{\eta \geq 0} \mathcal{O}_{\mathcal{L},\eta}(\mathcal{H})$ coincides with the set of aligned and uniform representations that maximize mutual information. We also connect our findings to sufficient dimension reduction in Appendix E.1.

We note that, in the concurrent work (Oko et al., 2025; Lin and Mei, 2025), sufficiency (Corollary 1) is obtained when there exists a pair of encoders that has infoNCE loss coinciding with the minimum over all similarity measures. In contrast, we consider the family of similarity measures taking the form

⁴See Appendix C.2 for the exact definition of $\varepsilon(\eta)$.



(a) Accuracy and intrinsic dimension with varying d . (b) Similarities and convergence of τ ($d = 20$).

Figure 3: Results with synthetic data: linear setting.

$S_\tau(U, V) = \tau^{-1}\sigma(U, V)$ adopted in CLIP and take into account the optimization of temperature, which is relevant to the result in Oord et al. (2018); Lin and Mei (2025) and Oko et al. (2025), but also reveals and explains new phenomena in practice, such as the convergence of temperature and the adaptation to intrinsic dimension. More importantly, our paper puts more emphasis on the exact statistical properties of learned representations, such as sufficiency and low-dimensionality that are shown in Theorem 2, while Oko et al. (2025); Lin and Mei (2025), through the sufficiency measure, focus on the bounds for downstream accuracy and the learnability (via excess infoNCE loss) of architectures (e.g., Transformers) under certain structured models.

4 Numerical experiments

In this section, we further justify the theoretical findings with both synthetic and real-world datasets. Starting with a synthetic dataset in Section 4.1, we further consider real datasets: a CITE-seq dataset (Stoeckius et al., 2017; Stuart et al., 2019) in Section 4.2, ImageNetV2 dataset (Recht et al., 2019) in Appendix G.6, and YFCC dataset (Thomee et al., 2016) in Appendix G.7. Throughout this section, we fit the representation map with a 5-layer ReLU neural network with middle-layer widths all fixed at 50 and the output space \mathbb{R}^d . This function class is denoted by $\mathcal{F}_{\text{NN}}^{p,d}$, where p is the input dimension adjusted for each setting. We estimate the global intrinsic dimension of data using the MLE-based approach proposed in Levina and Bickel (2004), which is implemented in the `skdim.id` package.⁵

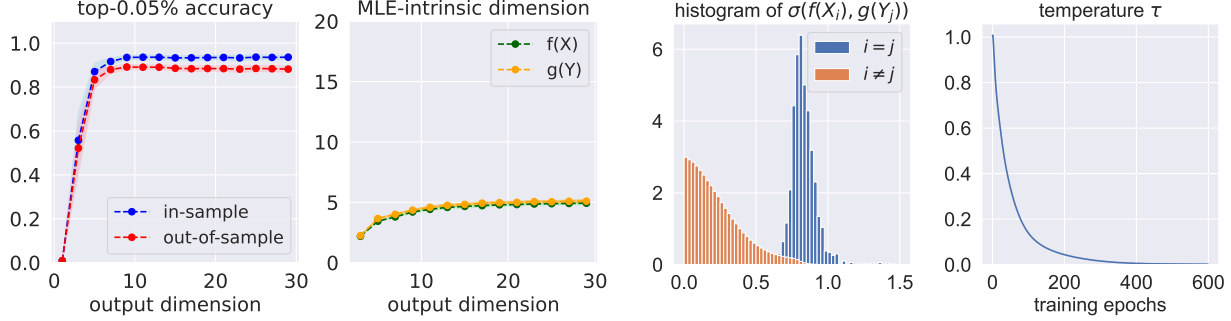
4.1 Results with synthetic data

We start with two synthetic datasets with $k^* < \min\{d_1, d_2\}$:

1. Linear setting: consider N i.i.d. draws from the same distribution shown in Section 1.1.
2. Nonlinear setting: consider N i.i.d. draws from the following distribution: $Y_i \stackrel{i.i.d.}{\sim} \mathcal{N}(0, \mathbf{I}_{d_2})$, $\xi_i \stackrel{i.i.d.}{\sim} \mathcal{N}(0, \mathbf{I}_{d_1-k^*})$, and $X_i = (0.2Y_{i1}^3, \sin(Y_{i2}Y_{i2}), \log(Y_{i3}^2), \dots, \log(Y_{ik^*}^2), \xi_i^\top)^\top$.

Here we set $d_1 = d_2 = 20$ and $k^* = 5$. The total $N = 14000$ data points are partitioned into a training set $\mathcal{D}_{\text{train}}$ with $|\mathcal{D}_{\text{train}}| = 10000$, a test set $\mathcal{D}_{\text{test}}$ with $|\mathcal{D}_{\text{test}}| = 2000$, and a separate set

⁵<https://scikit-dimension.readthedocs.io/en/latest/skdim.id.MLE.html>.



(a) Accuracy and intrinsic dimension with varying d . (b) Similarities and convergence of τ ($d = 20$).

Figure 4: Results with synthetic data: nonlinear setting.

with size 2000 for estimating the expected norm at each epoch. With representation maps $\hat{f} \in \mathcal{F}_{\text{NN}}^{d_1, d}$ and $\hat{g} \in \mathcal{F}_{\text{NN}}^{d_2, d}$ learned with $\mathcal{D}_{\text{train}}$, we consider the downstream task as the top- $\alpha\%$ matching of representations. More concretely, with $\mathcal{D} = \mathcal{D}_{\text{train}}$ or $\mathcal{D}_{\text{test}}$, for any $i \in \mathcal{D}$, denote $N_\alpha(i; \mathcal{D})$ as all the indices $j \in \mathcal{D}$ such that $\|\hat{f}(X_i) - \hat{g}(Y_j)\|$ is the $\lceil \alpha|\mathcal{D}| \rceil$ -smallest among $\|\hat{f}(X_i) - \hat{g}(Y_k)\|, k \in \mathcal{D}$, and accordingly,

$$\text{Acc}_\alpha(\mathcal{D}) = \frac{1}{|\mathcal{D}|} \sum_{i \in \mathcal{D}} \mathbb{1}\{i = N_\alpha(i; \mathcal{D})\}.$$

Then, we can define the in-sample and out-of-sample accuracy by $\text{Acc}_\alpha(\mathcal{D}_{\text{train}})$ and $\text{Acc}_\alpha(\mathcal{D}_{\text{test}})$, respectively. Particularly, with synthetic data, we choose $\alpha\% = 1/|\mathcal{D}_{\text{test}}| = 0.05\%$, which refers to the top-1 matching accuracy for out-of-sample matching.

Figures 3 and 4 report the results averaged over 50 repetitions in linear and nonlinear settings, respectively. We can see that in both settings, when the output dimension exceeds 5, both the in-sample and out-of-sample accuracy, and the MLE-based estimated intrinsic dimensions tend to saturate. Specifically, the estimated intrinsic dimensions approach the true value $k^* = 5$, which validates that minimizing the multi-modal contrastive loss automatically adapts to the underlying intrinsic dimension of data when the $d \geq k^*$. In addition, in each setting, we fix $d = 20$ and present the histogram of similarities as well as the convergence of τ in training in Figure 3b and Figure 4b, which validates the theoretical prediction that τ converges to zero and that the similarity measure between positive pairs will concentrate at a constant that dominates the similarity measure between negative pairs.

4.2 Results with CITE-seq dataset

The CITE-seq dataset contains simultaneous measurements of transcriptomes and cell-surface proteins from the same cell, and we get access to CITE-seq dataset via Seurat⁶ (Hao et al., 2021) in R. We focus on the CITE-seq healthy human bone marrow cells (BMCs) data, consisting of 30672 measured scRNA-seq profiles from bone marrow (Stuart et al., 2019), each with an additional panel of 25 antibodies. Following the preprocessing procedure in Seurat, we obtain a two-modal dataset with 24-dimensional protein data and 200-dimensional RNA data. More details of data preprocessing are presented in Appendix G.

⁶<https://satijalab.org/seurat/>.

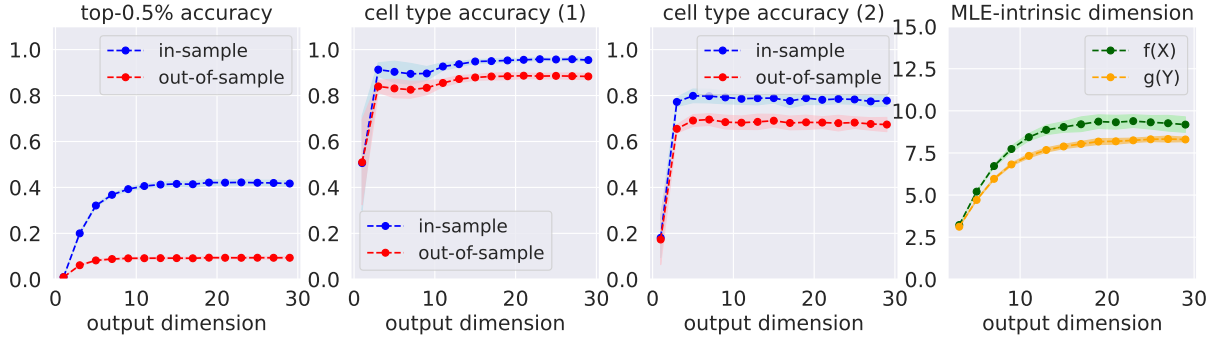


Figure 5: Results with CITE-seq dataset.

In each repetition of the experiments, we randomly sample 20000 rows without replacement from the preprocessed dataset and randomly split the subset into a training set $\mathcal{D}_{\text{train}}$ with $|\mathcal{D}_{\text{train}}| = 10000$, a test set $\mathcal{D}_{\text{test}}$ with $|\mathcal{D}_{\text{test}}| = 2000$, and a separate set with size 8000 for estimating the expected norm at each epoch. Representation maps $\hat{f}, \hat{g} \in \mathcal{F}_{\text{NN}}^{d_2, d}$ are learned with $\mathcal{D}_{\text{train}}$ via contrastive loss and the quality of representations is evaluated on $\mathcal{D}_{\text{test}}$ in terms of the classification accuracy of two groups of cell types and the top- $\alpha\%$ matching accuracy ($\alpha\% = 0.5\%$). We vary the output dimension d of the neural network architecture from 1 to 29, and results averaged after 50 repetitions with varying d are presented in Figure 5, in which, both in-sample and out-of-sample accuracy tend to saturate when the output dimension exceeds 10. In addition, in the right panel of Figure 5, the MLE-based estimated intrinsic dimension of in-sample representations does not exceed 10 regardless of the choice of output dimension. This demonstrates that the multi-modal contrastive loss effectively extracts intrinsically low-dimensional features from the CITE-seq dataset, which successfully capture the information to differentiate two levels of cell types. Moreover, as is shown in Appendix G.4, with different choices of output dimension d , the temperature tends to converge to zero in training, which offers evidence for the existence of nonempty $\mathcal{V}(\mathcal{H})$ when \mathcal{H} is a multi-layer ReLU network.

5 Related work

The integration of multi-modal data has been studied for decades in machine learning. The simplest practice is to concatenate features from all modalities, which is known as early fusion (Atrey et al., 2010), but the direct concatenation can lead to redundancy and high dimensionality (Nagrani et al., 2021). As a dimension reduction technique, canonical correlation analysis (CCA) (Harold, 1936; Anderson et al., 1958; Hotelling, 1992; Kettenring, 1971; Horst, 1961) is widely adopted to learn maximally correlated (linear) projections of modalities as the shared representation, which is further extended to nonlinear projections by kernel CCA (Akaho, 2006) and deep CCA (Andrew et al., 2013). With the initial purpose of integrating acoustic and visual speech signals (Yuhua et al., 1989; Partan and Marler, 1999), multi-modal learning has witnessed consistent progress in machine learning (Baltrušaitis et al., 2018). One line of research proposed fine-grained neural network architectures that can output joint representations of the multi-modal input (Mroueh et al., 2015; Ngiam et al., 2011; Silberer and Lapata, 2014). Another line of research adopts probabilistic graphical models with latent variables to characterize multi-modal data, such as multi-modal deep belief networks (Srivastava and Salakhutdinov, 2012a; Kim et al., 2013) and deep Boltzmann machines (Srivastava and Salakhutdinov,

2012b). Different architectures for modalities are also explored in the field, where certain (constrained) measures of cross-modal similarities are proposed for representation learning (Kiros et al., 2014; Zhang and Li, 2014; Pan et al., 2016).

Despite the wide applications of multi-modal learning, the theoretical understanding of its empirical success has drawn attention from the community only in recent years. Earlier works mainly interpret the advantage of multi-modalities from the information-theoretical perspective (Sridharan and Kakade, 2008; Federici et al., 2020; Liang et al., 2024). A recent work Huang et al. (2021) compares the generalization error with different subsets of modalities theoretically, and the result is further discussed in Lu (2023).

Similar to our scope, more recent papers include Uesaka et al. (2024), which focuses on the mutual information of multi-modal features as the upper bound of the additive inverse of contrastive loss, and Liu et al. (2024), which analyzes the solution of CLIP via the lens of independent component analysis (ICA) and depends on specific data generating process to ensure the identifiability. In addition, concurrent papers (Oko et al., 2025; Lin and Mei, 2025) introduce the notion of approximate sufficiency and show that this property is satisfied by learned representations by CLIP and also connect the sufficiency measure to the accuracy of downstream tasks with a goal similar to Chen et al. (2023).

6 Discussion

In this paper, we have characterized the statistical properties of learned representations in multi-modal contrastive learning, and specifically, have shown that the solution can adapt to the intrinsic dimension of data in the setting with $\mathcal{V}(\mathcal{H}) \neq \emptyset$. This property is also relevant to sufficient dimension reduction as is demonstrated in Appendix E.1. The theoretical result is also justified by both synthetic and real datasets, where the estimated intrinsic dimension as well as the downstream accuracy in various tasks tend to saturate regardless of the output dimension (once it exceeds the intrinsic dimension), which implies that the underlying information shared by modalities can indeed be captured by a low-dimensional structure. It is also worth noting that our theory suggests a two-stage fitting strategy when using CLIP. In the first stage, one selects a large output dimension so that the function class is expressive. In the second stage, one can use the intrinsic dimension discovered from the first stage and post-process the representation to a lower dimension. This could potentially accelerate the inference speed.

Our findings also suggest several future directions. Although $\mathcal{V}(\mathcal{H}) \neq \emptyset$ relaxes the condition in Wang and Isola (2020), it would be of theoretical interest for future work to characterize the precise limit of optimized temperature in general settings beyond this regime, which may also guide the practical choice of τ . In addition, it is interesting to study the finite-sample behavior of the infoNCE loss as well as its minimizers.

Acknowledgements

C.M. was partially supported by the National Science Foundation via grant DMS-2311127. Z.M. was partially supported by the National Science Foundation via grants DMS-2345215 and DMS-2245575.

References

- Akaho, S. (2006). A kernel method for canonical correlation analysis. *arXiv preprint cs/0609071*.
- Anderson, T. W., Anderson, T. W., Anderson, T. W., and Anderson, T. W. (1958). *An introduction to multivariate statistical analysis*, volume 2. Wiley New York.
- Andrew, G., Arora, R., Bilmes, J., and Livescu, K. (2013). Deep canonical correlation analysis. In *International conference on machine learning*, pages 1247–1255. PMLR.
- Argelaguet, R., Arnol, D., Bredikhin, D., Deloro, Y., Velten, B., Marioni, J. C., and Stegle, O. (2020). Mofa+: a statistical framework for comprehensive integration of multi-modal single-cell data. *Genome biology*, 21:1–17.
- Atrey, P. K., Hossain, M. A., El Saddik, A., and Kankanhalli, M. S. (2010). Multimodal fusion for multimedia analysis: a survey. *Multimedia systems*, 16:345–379.
- Bachman, P., Hjelm, R. D., and Buchwalter, W. (2019). Learning representations by maximizing mutual information across views. *Advances in neural information processing systems*, 32.
- Baltrušaitis, T., Ahuja, C., and Morency, L.-P. (2018). Multimodal machine learning: A survey and taxonomy. *IEEE transactions on pattern analysis and machine intelligence*, 41(2):423–443.
- Chen, Y., Jiao, Y., Qiu, R., and Yu, Z. (2024). Deep nonlinear sufficient dimension reduction. *The Annals of Statistics*, 52(3):1201–1226.
- Chen, Z., Deng, Y., Li, Y., and Gu, Q. (2023). Understanding transferable representation learning and zero-shot transfer in clip. *arXiv preprint arXiv:2310.00927*.
- Cook, R. D. (1996). Graphics for regressions with a binary response. *Journal of the American Statistical Association*, 91(435):983–992.
- Cook, R. D. and Li, B. (2002). Dimension reduction for conditional mean in regression. *The Annals of Statistics*, 30(2):455–474.
- Cover, T. M. (1999). *Elements of information theory*. John Wiley & Sons.
- Eshed, N. (2020). Novelty detection and analysis in convolutional neural networks. Master’s thesis, Cornell University.
- Federici, M., Dutta, A., Forré, P., Kushman, N., and Akata, Z. (2020). Learning robust representations via multi-view information bottleneck. *arXiv preprint arXiv:2002.07017*.
- Fukumizu, K., Bach, F. R., and Jordan, M. I. (2004). Dimensionality reduction for supervised learning with reproducing kernel hilbert spaces. *Journal of Machine Learning Research*, 5(Jan):73–99.
- Fukumizu, K., Bach, F. R., and Jordan, M. I. (2009). Kernel dimension reduction in regression.
- Galatolo, F. A., Cimino, M. G., and Vaglini, G. (2021). Generating images from caption and vice versa via clip-guided generative latent space search. *arXiv preprint arXiv:2102.01645*.

- Geiping, J., Garrido, Q., Fernandez, P., Bar, A., Pirsiavash, H., LeCun, Y., and Goldblum, M. (2023). A cookbook of self-supervised learning. *arXiv preprint arXiv:2304.12210*.
- Graves, L. M. (2012). *The theory of functions of real variables*. Courier Corporation.
- Gui, Y., Ma, C., and Zhong, Y. (2023). Unraveling projection heads in contrastive learning: Insights from expansion and shrinkage. *arXiv preprint arXiv:2306.03335*.
- Hao, Y., Hao, S., Andersen-Nissen, E., Mauck, W. M., Zheng, S., Butler, A., Lee, M. J., Wilk, A. J., Darby, C., Zager, M., et al. (2021). Integrated analysis of multimodal single-cell data. *Cell*, 184(13):3573–3587.
- HaoChen, J. Z., Wei, C., Gaidon, A., and Ma, T. (2021). Provable guarantees for self-supervised deep learning with spectral contrastive loss. *Advances in Neural Information Processing Systems*, 34:5000–5011.
- Harold, H. (1936). Relations between two sets of variables. *Biometrika*, 28(3):321–377.
- Hjelm, R. D., Fedorov, A., Lavoie-Marchildon, S., Grewal, K., Bachman, P., Trischler, A., and Bengio, Y. (2018). Learning deep representations by mutual information estimation and maximization. *arXiv preprint arXiv:1808.06670*.
- Horst, P. (1961). *Generalized canonical correlations and their application to experimental data*. Number 14. Journal of clinical psychology.
- Hotelling, H. (1992). Relations between two sets of variates. In *Breakthroughs in statistics: methodology and distribution*, pages 162–190. Springer.
- Huang, Y., Du, C., Xue, Z., Chen, X., Zhao, H., and Huang, L. (2021). What makes multi-modal learning better than single (provably). *Advances in Neural Information Processing Systems*, 34:10944–10956.
- Kettenring, J. R. (1971). Canonical analysis of several sets of variables. *Biometrika*, 58(3):433–451.
- Kim, H. J., Lin, Y., Geddes, T. A., Yang, J. Y. H., and Yang, P. (2020). Citefuse enables multi-modal analysis of cite-seq data. *Bioinformatics*, 36(14):4137–4143.
- Kim, Y., Lee, H., and Provost, E. M. (2013). Deep learning for robust feature generation in audio-visual emotion recognition. In *2013 IEEE international conference on acoustics, speech and signal processing*, pages 3687–3691. IEEE.
- Kiros, R., Salakhutdinov, R., and Zemel, R. S. (2014). Unifying visual-semantic embeddings with multimodal neural language models. *arXiv preprint arXiv:1411.2539*.
- Kraskov, A., Stögbauer, H., and Grassberger, P. (2004). Estimating mutual information. *Physical Review E—Statistical, Nonlinear, and Soft Matter Physics*, 69(6):066138.
- Laughlin, S. (1981). A simple coding procedure enhances a neuron’s information capacity. *Zeitschrift für Naturforschung c*, 36(9-10):910–912.
- Lee, J. M. and Lee, J. M. (2003). *Smooth manifolds*. Springer.

- Levina, E. and Bickel, P. (2004). Maximum likelihood estimation of intrinsic dimension. *Advances in neural information processing systems*, 17.
- Li, B., Artemiou, A., and Li, L. (2011). Principal support vector machines for linear and nonlinear sufficient dimension reduction.
- Li, B. and Song, J. (2017). Nonlinear sufficient dimension reduction for functional data.
- Li, K.-C. (1991). Sliced inverse regression for dimension reduction. *Journal of the American Statistical Association*, 86(414):316–327.
- Li, L. H., Yatskar, M., Yin, D., Hsieh, C.-J., and Chang, K.-W. (2019). Visualbert: A simple and performant baseline for vision and language. *arXiv preprint arXiv:1908.03557*.
- Li, Y., Liang, F., Zhao, L., Cui, Y., Ouyang, W., Shao, J., Yu, F., and Yan, J. (2021a). Supervision exists everywhere: A data efficient contrastive language-image pre-training paradigm. *arXiv preprint arXiv:2110.05208*.
- Li, Y., Pogodin, R., Sutherland, D. J., and Gretton, A. (2021b). Self-supervised learning with kernel dependence maximization. *Advances in Neural Information Processing Systems*, 34:15543–15556.
- Liang, P. P., Cheng, Y., Fan, X., Ling, C. K., Nie, S., Chen, R., Deng, Z., Allen, N., Auerbach, R., Mahmood, F., et al. (2024). Quantifying & modeling multimodal interactions: An information decomposition framework. *Advances in Neural Information Processing Systems*, 36.
- Lin, L. and Mei, S. (2025). A statistical theory of contrastive learning via approximate sufficient statistics. *arXiv preprint arXiv:2503.17538*.
- Liu, Y., Zhang, Z., Gong, D., Huang, B., Gong, M., Hengel, A. v. d., Zhang, K., and Shi, J. Q. (2024). Revealing multimodal contrastive representation learning through latent partial causal models. *arXiv preprint arXiv:2402.06223*.
- Lu, J., Batra, D., Parikh, D., and Lee, S. (2019). Vilbert: Pretraining task-agnostic visiolinguistic representations for vision-and-language tasks. *Advances in neural information processing systems*, 32.
- Lu, Z. (2023). A theory of multimodal learning. *Advances in Neural Information Processing Systems*, 36:57244–57255.
- Mroueh, Y., Marcheret, E., and Goel, V. (2015). Deep multimodal learning for audio-visual speech recognition. In *2015 IEEE International Conference on Acoustics, Speech and Signal Processing (ICASSP)*, pages 2130–2134. IEEE.
- Nagrani, A., Yang, S., Arnab, A., Jansen, A., Schmid, C., and Sun, C. (2021). Attention bottlenecks for multimodal fusion. *Advances in neural information processing systems*, 34:14200–14213.
- Nakada, R., Gulluk, H. I., Deng, Z., Ji, W., Zou, J., and Zhang, L. (2023). Understanding multimodal contrastive learning and incorporating unpaired data. In *International Conference on Artificial Intelligence and Statistics*, pages 4348–4380. PMLR.

- Nandy, S. and Ma, Z. (2024). Multimodal data integration and cross-modal querying via orchestrated approximate message passing. *arXiv preprint arXiv:2407.19030*.
- Ngiam, J., Khosla, A., Kim, M., Nam, J., Lee, H., and Ng, A. Y. (2011). Multimodal deep learning. In *Proceedings of the 28th international conference on machine learning (ICML-11)*, pages 689–696.
- Oko, K., Lin, L., Cai, Y., and Mei, S. (2025). A statistical theory of contrastive pre-training and multimodal generative ai. *arXiv preprint arXiv:2501.04641*.
- Oord, A. v. d., Li, Y., and Vinyals, O. (2018). Representation learning with contrastive predictive coding. *arXiv preprint arXiv:1807.03748*.
- Osgood, W. F. (1907). *Lehrbuch der funktionentheorie*, volume 20. BG Teubner.
- Pan, Y., Mei, T., Yao, T., Li, H., and Rui, Y. (2016). Jointly modeling embedding and translation to bridge video and language. In *Proceedings of the IEEE conference on computer vision and pattern recognition*, pages 4594–4602.
- Paninski, L. (2003). Estimation of entropy and mutual information. *Neural computation*, 15(6):1191–1253.
- Partan, S. and Marler, P. (1999). Communication goes multimodal. *Science*, 283(5406):1272–1273.
- Polyanskiy, Y. and Wu, Y. (2014). Lecture notes on information theory. *Lecture Notes for ECE563 (UIUC) and*, 6(2012-2016):7.
- Poole, B., Ozair, S., Van Den Oord, A., Alemi, A., and Tucker, G. (2019). On variational bounds of mutual information. In *International Conference on Machine Learning*, pages 5171–5180. PMLR.
- Radford, A., Kim, J. W., Hallacy, C., Ramesh, A., Goh, G., Agarwal, S., Sastry, G., Askell, A., Mishkin, P., Clark, J., et al. (2021). Learning transferable visual models from natural language supervision. In *International conference on machine learning*, pages 8748–8763. PMLR.
- Recht, B., Roelofs, R., Schmidt, L., and Shankar, V. (2019). Do imagenet classifiers generalize to imagenet? In *International conference on machine learning*, pages 5389–5400. PMLR.
- Ren, Y. and Li, Y. (2023). On the importance of contrastive loss in multimodal learning. *arXiv preprint arXiv:2304.03717*.
- Shi, P., Welle, M. C., Björkman, M., and Kragic, D. (2023). Towards understanding the modality gap in clip. In *ICLR 2023 Workshop on Multimodal Representation Learning: Perks and Pitfalls*.
- Silberer, C. and Lapata, M. (2014). Learning grounded meaning representations with autoencoders. In *Proceedings of the 52nd Annual Meeting of the Association for Computational Linguistics (Volume 1: Long Papers)*, pages 721–732.
- Sridharan, K. and Kakade, S. M. (2008). An information theoretic framework for multi-view learning. In *COLT*, number 114, pages 403–414.
- Srivastava, N. and Salakhutdinov, R. (2012a). Learning representations for multimodal data with deep belief nets. In *International conference on machine learning workshop*, volume 79, pages 978–1.

- Srivastava, N. and Salakhutdinov, R. R. (2012b). Multimodal learning with deep boltzmann machines. *Advances in neural information processing systems*, 25.
- Stoeckius, M., Hafemeister, C., Stephenson, W., Houck-Loomis, B., Chattopadhyay, P. K., Swerdlow, H., Satija, R., and Smibert, P. (2017). Simultaneous epitope and transcriptome measurement in single cells. *Nature methods*, 14(9):865–868.
- Stuart, T., Butler, A., Hoffman, P., Hafemeister, C., Papalexi, E., Mauck, W. M., Hao, Y., Stoeckius, M., Smibert, P., and Satija, R. (2019). Comprehensive integration of single-cell data. *cell*, 177(7):1888–1902.
- Tan, H. and Bansal, M. (2019). Lxmert: Learning cross-modality encoder representations from transformers. *arXiv preprint arXiv:1908.07490*.
- Teichmann, S. and Efremova, M. (2020). Method of the year 2019: single-cell multimodal omics. *Nat. Methods*, 17(1):2020.
- Thomee, B., Shamma, D. A., Friedland, G., Elizalde, B., Ni, K., Poland, D., Borth, D., and Li, L.-J. (2016). Yfcc100m: The new data in multimedia research. *Communications of the ACM*, 59(2):64–73.
- Tian, Y., Krishnan, D., and Isola, P. (2020). Contrastive multiview coding. In *Computer Vision—ECCV 2020: 16th European Conference, Glasgow, UK, August 23–28, 2020, Proceedings, Part XI 16*, pages 776–794. Springer.
- Tishby, N. and Zaslavsky, N. (2015). Deep learning and the information bottleneck principle. In *2015 IEEE information theory workshop (itw)*, pages 1–5. Ieee.
- Tschannen, M., Djolonga, J., Rubenstein, P. K., Gelly, S., and Lucic, M. (2019). On mutual information maximization for representation learning. *arXiv preprint arXiv:1907.13625*.
- Uesaka, T., Suzuki, T., Takida, Y., Lai, C.-H., Murata, N., and Mitsufuji, Y. (2024). Understanding multimodal contrastive learning through pointwise mutual information. *arXiv preprint arXiv:2404.19228*.
- Van Erven, T. and Harremos, P. (2014). Rényi divergence and kullback-leibler divergence. *IEEE Transactions on Information Theory*, 60(7):3797–3820.
- Wang, F. and Liu, H. (2021). Understanding the behaviour of contrastive loss. In *Proceedings of the IEEE/CVF conference on computer vision and pattern recognition*, pages 2495–2504.
- Wang, T. and Isola, P. (2020). Understanding contrastive representation learning through alignment and uniformity on the hypersphere. In *International conference on machine learning*, pages 9929–9939. PMLR.
- Xia, Y. (2008). A multiple-index model and dimension reduction. *Journal of the American Statistical Association*, 103(484):1631–1640.
- Xu, P., Zhu, X., and Clifton, D. A. (2023). Multimodal learning with transformers: A survey. *IEEE Transactions on Pattern Analysis and Machine Intelligence*, 45(10):12113–12132.

- Yuhas, B. P., Goldstein, M. H., and Sejnowski, T. J. (1989). Integration of acoustic and visual speech signals using neural networks. *IEEE Communications Magazine*, 27(11):65–71.
- Zhang, D. and Li, W.-J. (2014). Large-scale supervised multimodal hashing with semantic correlation maximization. In *Proceedings of the AAAI conference on artificial intelligence*, volume 28.
- Zimmermann, R. S., Sharma, Y., Schneider, S., Bethge, M., and Brendel, W. (2021). Contrastive learning inverts the data generating process. In *International Conference on Machine Learning*, pages 12979–12990. PMLR.

Contents

A Preliminaries	21
A.1 Notations	21
A.2 Discretization of \tilde{B}_d	21
A.2.1 A fine-grained order	22
A.2.2 Approximation by discretization	22
A.3 Intrinsic dimension and its properties	24
A.3.1 Proof of Lemma 6	24
B Properties of $\mathcal{V}(\mathcal{H})$	25
B.1 Proof of Lemma 7 (1)	26
B.2 Proof of Lemma 7 (2)	27
C Properties of infoNCE loss	28
C.1 A decomposition of the infoNCE loss	28
C.1.1 Proof of Lemma 8	29
C.2 Properties of (approximate) minimizers	30
C.2.1 Proof of Lemma 9	31
C.2.2 Proof of Lemma 10 (1) and (2)	33
C.2.3 Proof of Lemma 10 (3)	34
D Proof of Theorem 2	35
D.1 Proof of Step 1	36
D.2 Proof of Step 2	37
E Extensions and additional theoretical results	39
E.1 Connection with sufficient dimension reduction	39
E.1.1 Proof of Proposition 2	40
E.1.2 Extension of Proposition 2	40
E.2 Alignment and uniformity with correctly specified dimension	41
E.2.1 Proof of Theorem 3	42
F Proof of preliminary results in Section A.2	42
F.1 Proof of Lemma 1	42
F.2 Proof of Lemma 3	42
F.3 Proof of Lemma 4	44
F.4 Proof of Lemma 5	45
G Additional experimental results	45
G.1 Norm concentration	46
G.2 Example with $\mathcal{V}(\mathcal{H}) = \emptyset$: alignment versus simply similarity maximization	46
G.3 Experiment setup	47
G.4 Convergence of temperature	48
G.5 Comparison with cosine similarity	48
G.6 Results with ImageNetV2 dataset	49

G.7 Results with YFCC dataset 50

A Preliminaries

We start with preliminaries, including notations and the discretization of \tilde{B}_d introduced in Section 2.1.

A.1 Notations

We start by summarizing important notations in Table 1.

\mathbb{R}^d	d -dimensional Eudclidean space
\tilde{B}_d	$\{x \in \mathbb{R}^d : \ x\ \leq \sqrt{\Omega}\}$
$\text{ID}(f)$	intrinsic dimension of f (Definition 3)
$C_M = \{c_{M,i} : i \in [M]\}$	a disjoint partition of \tilde{B}_d
$\hat{\mathcal{B}}_{d,M} = \{z_{M,i} \in c_{M,i} : i \in [M]\}$	discretization of $\tilde{\mathcal{B}}_d$ under C_M
f_M, g_M	discretizations of $(f, g) \in \mathcal{H}$
\mathcal{H}_M	$\{(f_M, g_M) : (f, g) \in \mathcal{H}\}$
$m_\sigma(f, g)$	$\text{ess sup}_{X \perp\!\!\!\perp \tilde{Y}} \sigma(f(X), g(\tilde{Y}))$
$\mathcal{A}(\mathcal{H}')$	$\{(f, g) \in \mathcal{H}' : \frac{f(X)}{\mathbb{E}\ f(X)\ } = \frac{g(Y)}{\mathbb{E}\ g(Y)\ } \text{ a.s. and } m_\sigma(f, g) = 1\}$
$I_M^*(\mathcal{H})$	$\sup_{(f,g) \in \mathcal{H}} I(f_M(X), g_M(Y))$
$\mathcal{W}(\mathcal{H}')$	$\{(f, g) \in \mathcal{H}' : \liminf_{M \rightarrow +\infty} (I(f_M(X); g_M(Y)) - I_M^*(\mathcal{H})) \geq 0\}$
$\mathcal{V}(\mathcal{H}')$	$\mathcal{A}(\mathcal{H}') \cap \mathcal{W}(\mathcal{H}')$
$Q_{f(X),g(Y),\tau}, \tilde{Q}_{f(X),g(Y),\tau}$	smoothed distributions defined in (6)
$Q_{f(X),g(Y),\tau}^M = Q_\tau^M, \tilde{Q}_{f(X),g(Y),\tau}^M = \tilde{Q}_\tau^M$	discretized distributions defined with (f_M, g_M)
$\varepsilon(\eta)$	temperature threshold with tolerance η defined in (9)
$O_{\mathcal{L},\varepsilon,\eta}(\mathcal{H})$ (7)	Set of minimizers up to tolerance τ with temperature threshold ε
$O_{\mathcal{L},\eta}(\mathcal{H})$ (3)	Set of minimizers up to tolerance τ with temperature threshold $\varepsilon(\eta)$

Table 1: Table of notations

A.2 Discretization of \tilde{B}_d

With the defined similarity measure $\sigma(\cdot, \cdot)$, to analyze the mutual information between $f(X)$ and $g(Y)$, it is equivalent to considering mutual information between $\tilde{f}(X) = f(X)/\mathbb{E}\|f(X)\|$ and $\tilde{g}(Y) = g(Y)/\mathbb{E}\|g(Y)\|$, which satisfies $\mathbb{E}\|\tilde{f}(X)\| = \mathbb{E}\|\tilde{g}(Y)\| = 1$, $\|\tilde{f}(X)\|, \|\tilde{g}(Y)\| \leq \sqrt{\Omega} < \infty$ almost surely. Then, we denote the range of normalized representations by \tilde{B}_d , which is compact.

For any fineness $M \in \mathcal{M} \subseteq \mathbb{N}$, we consider a discretization $C_M = \{c_{M,i}\}_{i \in [M]}$ of \tilde{B}_d such that the compact set \tilde{B}_d is divided into M connected portions, and representatives from each portion $c_{M,i}$ form

the set $\widehat{\mathcal{B}}_{d,M} = \{z_{M,i}\}_{i \in [M]}$. We also denote \mathcal{C}_M as the set of all discretizations C_M of \widetilde{B}_d such that

$$\max_{i \in [M]} \text{diam}(c_{M,i}) \rightarrow 0 \quad \text{as} \quad M \rightarrow +\infty.$$

Particularly, we consider the discretization $C_M \in \mathcal{C}_M$ such that each portion $c_{M,i}$ has the same Lebesgue measure Δ_M , which satisfies $\lim_{M \rightarrow +\infty} \Delta_M = 0$. In addition, we assume the sequence of discretizations $\{C_M\}_{M \in \mathcal{M}}$ is nested such that $C_{M'} \subseteq C_M$ for any $M' \leq M$.

In the rest of the proof, we write $M \rightarrow +\infty$ to denote $\mathcal{M} \ni M \rightarrow +\infty$. Accordingly, for any function f , we define

$$f_M(x) = z_{M,i} \quad \text{if } x \in f^{-1}(c_{M,i}),$$

and the function class $\mathcal{H}_M = \{(f_M, g_M) : (f, g) \in \mathcal{H}\}$, which is also nested in the sense that $\mathcal{H}_M \subseteq \mathcal{H}_{\widetilde{M}}$ for all $M \leq \widetilde{M}$. We also notice that \mathcal{H}_M can be viewed as the class of piecewise constant functions. For any $1 \leq k \leq d$, the set \mathcal{H}_M^k is defined similarly.

Abusing notations, for any random vector U supported on \widetilde{B}_d , we write $U_M = U(\widehat{\mathcal{B}}_{d,M})$ to denote the discretization of U , for which

$$\mathbb{P}(U_M = z_{M,i}) = \mathbb{P}(U \in c_{M,i}) \quad \text{and} \quad \mathbb{P}(U_M \notin \widehat{\mathcal{B}}_{d,M}) = 0.$$

If U is supported on $\widehat{\mathcal{B}}_{d,M}$, we have $U_M = U$ almost surely and, particularly, $f_M(X) = (f(X))_M$ almost surely.

A.2.1 A fine-grained order

For any pairs of random vectors $U = (U_1, \dots, U_l), \widetilde{U} = (\widetilde{U}_1, \dots, \widetilde{U}_l) \in (\widetilde{B}_d)^l$ and any functional G of random vectors, we define the order $\preceq_{\mathcal{M}}$ as follows.

$$G(U) \preceq_{\mathcal{M}} G(\widetilde{U}) \iff \limsup_{M \rightarrow +\infty} \left\{ G(U_M) - G(\widetilde{U}_M) \right\} \leq 0,$$

and moreover, the inequality is strict, i.e. $G(U) \prec_{\mathcal{M}} G(\widetilde{U})$, if and only if

$$\limsup_{M \rightarrow +\infty} \left\{ G(U_M) - G(\widetilde{U}_M) \right\} < 0.$$

We also write $G(U) =_{\mathcal{M}} G(\widetilde{U})$ if $\lim_{M \rightarrow +\infty} \left\{ G(U_M) - G(\widetilde{U}_M) \right\}$ exists and is zero.

A.2.2 Approximation by discretization

In this section, we study the properties of the aforementioned discretization. To start with, for a discrete random vector U with the probability mass function p_U , we define the entropy of U by $H(U) = -\mathbb{E}[\log p_U(U)]$. For a continuous random vector U with probability density function p_U , we define the differential entropy of U by $\widetilde{H}(U) = -\mathbb{E}[\log p_U(U)]$.

Approximation of entropy and relative entropy. To start with, consider the random vector $U \in \widetilde{B}_d$ with probability density function p and the discretized random variable $U_M \in \widetilde{B}_d$ such that $p_i = \mathbb{P}(U_M = z_{M,i}) = \mathbb{P}(U \in c_{M,i})$. As $\int_{c_{M,i}} p(u) du \approx p(z_{M,i}) \Delta_M$, we have the following result that connects the Shannon entropy of U_M and the differential entropy of U .

Lemma 1. ([Cover, 1999, Theorem 8.3.1](#)) As $M \rightarrow +\infty$ and $\text{diam}(c_{M,i}) \rightarrow 0$, it holds that

$$\lim_{M \rightarrow +\infty} (H(U_M) + \log \Delta_M) = \tilde{H}(U).$$

See proof in Section [F](#).

In addition, for two random vectors U, V supported on \tilde{B}_d , we recall ([Van Erven and Harremos, 2014, Theorem 21](#)) in the following lemma.

Lemma 2. ([Van Erven and Harremos, 2014, Theorem 21](#)) For any $C_M \in \mathcal{C}_M$ with $M \rightarrow +\infty$ and $\text{diam}(c_{M,i}) \rightarrow 0$, it holds that for any M ,

$$D_{\text{KL}}(U_M \parallel V_M) \leq D_{\text{KL}}(U_{M+1} \parallel V_{M+1}) \leq D_{\text{KL}}(U \parallel V),$$

and moreover,

$$\lim_{M \rightarrow +\infty} D_{\text{KL}}(U_M \parallel V_M) = D_{\text{KL}}(U \parallel V).$$

Approximation of conditional entropy. For later use, we also consider the approximation of the following quantity

$$\tilde{H}(\phi(U, V) \mid U),$$

where U, V are random vectors on \tilde{B}_d with joint density $p(u, v)$ and $\phi : \tilde{B}_d \times \tilde{B}_d \rightarrow \mathbb{R}$ is continuous. We have the following result.

Lemma 3. Assume $\phi : \tilde{B}_d \times \tilde{B}_d \rightarrow \mathbb{R}$ is continuous. For any $C_M \in \mathcal{C}_M$ with $M \rightarrow +\infty$ and $\text{diam}(c_{M,i}) \rightarrow 0$, if $\tilde{H}(\phi(U, V) \mid U) > 0$, it holds that

$$\liminf_{M \rightarrow +\infty} H(\phi(U_M, V_M) \mid U_M) > 0.$$

See proof in Section [F](#).

Approximation of (conditional) mutual information. Consider random vectors U, V on \tilde{B}_d and continuous maps $\phi, \psi : \tilde{B}_d \times \tilde{B}_d \rightarrow \mathbb{R}$. We are interested in the approximation of $I(\phi(U, V); \psi(U, V))$ and $I(\phi(U, V); \psi(U, V) \mid U)$ by its discretized version. To start with, we have the following result.

Lemma 4. Assume ϕ and ψ are continuous and $\mathbb{P}(\phi(U, V) = \psi(U, V)) < 1$. For any $C_M \in \mathcal{C}_M$ with $M \rightarrow +\infty$ and $\text{diam}(c_{M,i}) \rightarrow 0$, it holds that

$$\lim_{M \rightarrow +\infty} I(\phi(U_M, V_M); \psi(U_M, V_M)) = I(\phi(U, V); \psi(U, V)).$$

See proof in Section F.

For the conditional mutual information, note that

$$I(\phi(U, V); \psi(U, V) \mid U) = I(\phi(U, V); \psi(U, V), U) - I(\phi(U, V); U).$$

Lemma 4 can be applied to both terms, which indicates that

$$\lim_{M \rightarrow +\infty} I(\phi(U_M, V_M); \psi(U_M, V_M) \mid U_M) = I(\phi(U, V); \psi(U, V) \mid U).$$

Related results on estimating mutual information based on discretization and binning can be found in Kraskov et al. (2004); Paninski (2003); Cover (1999).

Approximation of infoNCE loss. For any pair of representation maps $(f, g) \in \mathcal{H}$, we have the following result.

Lemma 5. *For any $(f, g) \in \mathcal{H}$ with $\mathbb{E}\|f(X)\| = \mathbb{E}\|g(Y)\| = 1$ and any $\tau > 0$, it holds that*

$$\lim_{M \rightarrow +\infty} \mathcal{L}(f_M, g_M, \tau) = \mathcal{L}(f, g, \tau).$$

See proof in Section F.

A.3 Intrinsic dimension and its properties

We revisit the definition of intrinsic dimension in Definition 3 for which we have the following property for $\text{ID}(f)$.

Lemma 6. *Suppose $f : \mathbb{R}^{d_1} \rightarrow \mathbb{R}^d$ satisfies $\text{ID}(f) = k$. Then, for any measurable function $\psi : \mathbb{R}^d \rightarrow \mathbb{R}^d$, it holds that $\text{ID}(\psi \circ f) \leq k$.*

A.3.1 Proof of Lemma 6

Suppose $\text{ID}(f) = k$. Then, by Definition 3, there exist a measurable function $h : \mathbb{R}^{d_1} \rightarrow \mathbb{R}^d$ with $\dim(R(h)) = k$ and an injective function $\phi : \mathbb{R}^d \rightarrow \mathbb{R}^d$ such that $f = \phi \circ h$.

For any measurable function $\psi : \mathbb{R}^d \rightarrow \mathbb{R}^d$, if ψ is injective, then $\phi \circ f = (\psi \circ \phi) \circ h$. Since $\psi \circ \phi$ is injective, by definition, we have $\text{ID}(\psi \circ f) = k$.

If ψ is not injective, for any $x \in \mathbb{R}^{d_1}$, define

$$\mathcal{T}(x) = \{x' : (\psi \circ \phi \circ h)(x') = (\psi \circ \phi \circ h)(x)\},$$

and accordingly, we define the equivalence relation \sim : $x \sim x'$ if and only if $\mathcal{T}(x) = \mathcal{T}(x')$, with which $\Pi(x) = \{x' : x' \sim x\}$. Then, denote x/\sim as the representative of $\Pi(x)$. Based on the notations above, define

$$\tilde{h} : x \mapsto h(x/\sim).$$

We can verify that for any $x \in \mathbb{R}^{d_1}$, it holds that

$$(\psi \circ \phi \circ h)(x) = (\psi \circ \phi \circ h)(x/\sim) = (\psi \circ \phi \circ \tilde{h})(x).$$

In addition, for any $z_1, z_2 \in R(\phi \circ \tilde{h})$, it holds that $\psi(z_1) \neq \psi(z_2)$. Otherwise, suppose there exist $z_1 \neq z_2 \in R(\phi \circ \tilde{h})$, i.e., there exist $x_1, x_2 \in \mathbb{R}^{d_1}$ satisfying $z_i = (\phi \circ \tilde{h})(x_i)$ with $i \in \{1, 2\}$, such that $\psi(z_1) = \psi(z_2)$. Then, by the definition of the equivalence relation \sim and the definition of \tilde{h} , we obtain $x_1 \sim x_2$, thus $x_1/\sim = x_2/\sim$ and

$$z_1 = (\phi \circ \tilde{h})(x_1) = (\phi \circ \tilde{h})(x_2) = z_2,$$

which draws the contradiction. Hence, $\psi|_{R(\phi \circ \tilde{h})}$, i.e., ψ restricted on the range of $\phi \circ \tilde{h}$ is injective. Then, $(\psi \circ \phi)|_{R(\tilde{h})}$ is also injective. Consequently, we have constructed an injective map $(\psi \circ \phi)|_{R(\tilde{h})}$ and a measurable function \tilde{h} with $\dim(R(\tilde{h})) \leq \dim(R(h)) = k$ such that

$$(\psi \circ f)(x) = [(\psi \circ \phi) \circ \tilde{h}](x) \quad \text{almost everywhere,}$$

which, by Definition 3, implies that $\text{ID}(\psi \circ f) \leq \text{ID}(f) = k$.

B Properties of $\mathcal{V}(\mathcal{H})$

In this section, we focus on the properties of the set $\mathcal{V}(\mathcal{H})$. To begin with, for any subset $\mathcal{H}' = \mathcal{H}'_X \times \mathcal{H}'_Y \subseteq \mathcal{H}$, we generalize the definitions of $\mathcal{A}(\mathcal{H})$ and $\mathcal{W}(\mathcal{H})$ as follows.

Definition 4. We define the set of representation maps that realize alignment and similarity maximization as

$$\mathcal{A}(\mathcal{H}') = \left\{ (f, g) \in \mathcal{H}' : \frac{f(X)}{\mathbb{E}\|f(X)\|} = \frac{g(Y)}{\mathbb{E}\|g(Y)\|} \text{ almost surely and } m_\sigma(f, g) = 1 \right\}.$$

Here $m_\sigma(f, g) := \text{ess sup}_{X \perp\!\!\!\perp \tilde{Y}} \sigma(f(X), g(\tilde{Y}))$ for any $(f, g) \in \mathcal{H}$.

Definition 5 (Maximal mutual information). We define the following set of pairs $(f, g) \in \mathcal{H}$ that sufficiently capture the dependence between X and Y :

$$\mathcal{W}(\mathcal{H}') = \{(f, g) \in \mathcal{H}' : \liminf_{M \rightarrow +\infty} (I(f_M(X); g_M(Y)) - I_M^*(\mathcal{H})) \geq 0\},$$

where $I_M^*(\mathcal{H}) = \sup_{(f, g) \in \mathcal{H}} I(f_M(X); g_M(Y))$.

Note that in the definition of $\mathcal{W}(\mathcal{H}')$ for any $\mathcal{H}' \subseteq \mathcal{H}$, the benchmark mutual information $I^*(\mathcal{H})$ is defined for the entire class \mathcal{H} . Accordingly, we define $\mathcal{V}(\mathcal{H}') = \mathcal{A}(\mathcal{H}') \cap \mathcal{W}(\mathcal{H}')$.

Then, we are ready to present the following lemma on properties of $\mathcal{V}(\mathcal{H})$.

Lemma 7. Assume $\mathcal{V}(\mathcal{H}) \neq \emptyset$. There exists $k^* \in [d]$ such that for any $(f^*, g^*) \in \mathcal{V}(\mathcal{H})$,

(1) *Intrinsic dimension adaptation.* $\text{ID}(f^*) = \text{ID}(g^*) = k^*$.

(2) *Sufficiency.* If $k^* < d$, for any $(f, g) \in \mathcal{H}$ with $\max\{\text{ID}(f), \text{ID}(g)\} > k^*$, it holds that

$$f(X) \perp\!\!\!\perp g(Y) \mid f^*(X).$$

See proof in Section B.1 and Section B.2, respectively. We note that Proposition 1 is directly implied by Lemma 7 (1).

B.1 Proof of Lemma 7 (1)

To start with, for any integer $k \in [d]$, we define $\mathcal{H}^k = \{(f, g) \in \mathcal{H} : \text{ID}(f) = \text{ID}(g) = k\}$ and $\mathcal{V}(\mathcal{H}^k)$ is defined accordingly by

$$\mathcal{V}(\mathcal{H}^k) = \{(f, g) \in \mathcal{V}(\mathcal{H}) : \text{ID}(f) = \text{ID}(g) = k\}.$$

Then, we define

$$\tilde{k} = \max \left\{ k \in [d] : \mathcal{V}(\mathcal{H}^k) \neq \emptyset \right\}.$$

By definitions of $\mathcal{V}(\mathcal{H})$ and $\mathcal{V}(\mathcal{H}^k)$, we have $\mathcal{V}(\mathcal{H}^{\tilde{k}}) \subseteq \mathcal{V}(\mathcal{H})$, and we will show that $\mathcal{V}(\mathcal{H}) \subseteq \mathcal{V}(\mathcal{H}^{\tilde{k}})$.

Case 1. If $\tilde{k} = 1$, recall the definition of $\tilde{k} = \max\{k \in [d] : \mathcal{V}(\mathcal{H}^k) \neq \emptyset\}$. For any $(f, g) \in \mathcal{V}(\mathcal{H})$, suppose $\text{ID}(f) = k > 1$, it holds that $(f, g) \in \mathcal{H}^k$, thus $\tilde{k} \geq k > 1$, which draws the contradiction. Hence, for any $(f, g) \in \mathcal{V}(\mathcal{H})$, we have $(f, g) \in \mathcal{H}^1$, i.e. $\mathcal{V}(\mathcal{H}^{\tilde{k}}) = \mathcal{V}(\mathcal{H})$.

Case 2. Consider the case with $\tilde{k} > 1$. Suppose there exist $(f^*, g^*) \in \mathcal{V}(\mathcal{H}^{\tilde{k}})$ and $(f, g) \in \mathcal{V}(\mathcal{H}^k)$ but $k < \tilde{k} \leq d$. Since both mutual information and infoNCE loss are scale-invariant with respect to both f and g , without loss of generality, we assume $\mathbb{E}\|f(X)\| = \mathbb{E}\|g(Y)\| = \mathbb{E}\|f^*(X)\| = \mathbb{E}\|g^*(X)\| = 1$. Then, since $\max\{\text{ID}(f), \text{ID}(g)\} = k < \tilde{k} \leq d$, by Definition 3, there exist aligned $F(X), G(Y) \in \mathbb{R}^k$ and injective measurable functions $\phi, \psi : \mathbb{R}^k \rightarrow \mathbb{R}^d$ such that

$$f(X) = \phi(F(X)) \quad g(Y) = \psi(G(Y)).$$

Here we define $H(U)$ as the entropy of random vector U and $U_M = \text{id}_M(U)$, where id is the identical map on \mathbb{R}^d . Then, there exists $\Psi : \mathbb{R}^d \times \mathbb{R}^d \rightarrow \mathbb{R}$ such that

$$0 < \tilde{H}(\Psi(f^*(X), f(X)) \mid f(X)).$$

Otherwise, there exists a measurable function ζ such that $f^*(X) = \zeta(f(X))$ almost surely. By Definition 3, it holds that $\text{ID}(f) \leq \text{ID}(f^*) = \tilde{k} < k$, which draws the contradiction.

Then, as $\tilde{H}(\Psi(f^*(X), f(X)) \mid f(X)) = \tilde{H}(\Psi(f^*(X), f(X)), f(X)) - \tilde{H}(f(X))$, by Lemma 3, we also have

$$0 \prec_{\mathcal{M}} H(\Psi(f^*(X), f(X)) \mid f(X)).$$

Otherwise, for any Ψ , it holds that $\Psi(f^*(X), f(X))$ is a deterministic function of $f(X)$. Specifically, $f^*(X)$ is a function of $f(X)$ and by Definition 3, we obtain $\tilde{k} = \text{ID}(f^*) \leq \text{ID}(f) = k$, which draws the contradiction.

Hence, we can define

$$\bar{F}(X) = \begin{pmatrix} F(X) \\ \mathbf{0}_{d-k-1} \\ \Psi(f(X), f^*(X)) \end{pmatrix} \quad \text{and} \quad \bar{G}(Y) = \begin{pmatrix} G(Y) \\ \mathbf{0}_{d-k-1} \\ \Psi(g(Y), g^*(Y)) \end{pmatrix},$$

with which

$$\begin{aligned} -I(\bar{F}(X); \bar{G}(Y)) &=_{\mathcal{M}} -H(\bar{F}(X)) \\ &=_{\mathcal{M}} -H(F(X)) - H(\Psi(f^*(X), f(X)) \mid F(X)) \\ &\prec_{\mathcal{M}} -H(F(X)) \\ &=_{\mathcal{M}} -I(F(X); G(Y)). \end{aligned}$$

Since ϕ and ψ are injective, we further have

$$-I(\bar{F}(X); \bar{G}(Y)) \prec_{\mathcal{M}} -I(F(X); G(Y)) =_{\mathcal{M}} -I(f(X); g(Y)),$$

which contradicts the fact that $(f, g) \in \mathcal{W}(\mathcal{H})$, which completes the proof. Hence, in the remaining part of the proof, we can define $k^* = \tilde{k}$.

B.2 Proof of Lemma 7 (2)

Suppose the statement is not true. Then, there exists $\tilde{\Phi}_1, \tilde{\Phi}_2 : \mathbb{R}^d \times \mathbb{R}^d \rightarrow \mathbb{R}$ such that

$$0 < I(\tilde{\Phi}_1(f(X), f^*(X)); \tilde{\Phi}_2(g(Y), g^*(Y)) \mid f^*(X)),$$

which, by Lemma 4, further indicates that

$$0 \prec_{\mathcal{M}} I(\tilde{\Phi}_1(f(X), f^*(X)); \tilde{\Phi}_2(g(Y), g^*(Y)) \mid f^*(X)). \quad (4)$$

To see this, if the statement is not true, it holds that for any $\tilde{\Phi}_1, \tilde{\Phi}_2 : \mathbb{R}^d \times \mathbb{R}^d \rightarrow \mathbb{R}$,

$$\tilde{\Phi}_1(f(X), f^*(X)) \perp\!\!\!\perp \tilde{\Phi}_2(g(Y), g^*(Y)) \mid f^*(X).$$

Specifically, we have $f(X) \perp\!\!\!\perp g(Y) \mid f^*(X)$, which draws the contradiction.

Since $k^* < d$, there exist injective measurable functions $\phi^*, \psi^* : \mathbb{R}^{k^*} \rightarrow \mathbb{R}^d$ and $F^*(X), G^*(Y) \in \mathbb{R}^{k^*}$ such that

$$f^*(X) = \phi^*(F^*(X)) \quad g^*(Y) = \psi^*(G^*(Y)).$$

Then, we can define

$$\check{F}(X) = \begin{pmatrix} F^*(X) \\ \mathbf{0}_{d-k^*-1} \\ \tilde{\Phi}_1(f(X), f^*(X)) \end{pmatrix} \quad \text{and} \quad \check{G}(Y) = \begin{pmatrix} G^*(Y) \\ \mathbf{0}_{d-k^*-1} \\ \tilde{\Phi}_2(g(Y), g^*(Y)) \end{pmatrix},$$

with which, we have

$$-I(\tilde{F}(X); \tilde{G}(Y)) \preceq_{\mathcal{M}} -I(F^*(X); \tilde{G}(Y)) \preceq_{\mathcal{M}} -I(F^*(X); G^*(Y)).$$

Here $=_{\mathcal{M}}$ holds in the first inequality if and only if $\tilde{G}(Y) \perp\!\!\!\perp \tilde{\Phi}_1(f(X), f^*(X)) \mid F^*(X)$, i.e.

$$\tilde{\Phi}_2(g(Y), g^*(Y)) \perp\!\!\!\perp \tilde{\Phi}_1(f(X), f^*(X)) \mid f^*(X),$$

which draws the contradiction to the construction of $\tilde{\Phi}_1$ and $\tilde{\Phi}_2$ in (4). Since ϕ^* and ψ^* are injective, we further obtain

$$-I(\tilde{F}(X); \tilde{G}(Y)) \prec_{\mathcal{M}} -I(f^*(X); g^*(Y)),$$

which draws the contradiction to the fact that $(f^*, g^*) \in \mathcal{W}(\mathcal{H})$. Thus, we obtain

$$f(X) \perp\!\!\!\perp g(Y) \mid f^*(X).$$

C Properties of infoNCE loss

Before presenting the technical proof of the main results on intrinsic dimension adaptation, we summarize some properties of the infoNCE loss.

C.1 A decomposition of the infoNCE loss

A pillar of our proof is the following decomposition of the infoNCE loss that characterizes the gap between the infoNCE loss and mutual information. Similar decompositions have appeared in (Oord et al., 2018; Wang and Isola, 2020; Oko et al., 2025).

Lemma 8. *Let $(f(X), g(Y)) \sim P_{f(X), g(Y)}$. If $I(f(X), g(Y)) < +\infty$, there exist joint distributions $Q_{f(X), g(Y), \tau}$ and $\tilde{Q}_{f(X), g(Y), \tau}$ such that $\mathcal{L}(f, g, \tau)$ can be decomposed as*

$$-2I(f(X); g(Y)) + D_{\text{KL}}(P_{f(X), g(Y)} \parallel Q_{f(X), g(Y), \tau}) + D_{\text{KL}}(P_{f(X), g(Y)} \parallel \tilde{Q}_{f(X), g(Y), \tau}). \quad (5)$$

The formal definitions of $Q_{f(X), g(Y), \tau}$ and $\tilde{Q}_{f(X), g(Y), \tau}$ are presented in Appendix C.1.1. In short, they can be viewed as the kernel smoothing of $P_{f(X), g(Y)}$ in the product space.

Conceptually, given the decomposition (5), minimizing the infoNCE loss is equivalent to simultaneously maximizing the mutual information between $f(X)$ and $g(Y)$, and minimizing the KL-divergence between $P_{f(X), g(Y)}$ and its smoothed versions. Here, the latter encourages the joint distribution of $P_{f(X), g(Y)}$ to spread across the support and implicitly enforces uniformity of the distribution $P_{f(X), g(Y)}$, which is in line with Wang and Isola (2020). In our actual proof, the lemma will be used together with discretizations introduced in Section 2.1 and (3) that ensure the finiteness of mutual information.

This decomposition is also relevant to the analysis in Oord et al. (2018); Oko et al. (2025), where the minimum of infoNCE loss over all possible similarity measures is shown to be bounded from below by $-2I(f(X); g(Y))$. However, in our paper, we focus on the inner product-based similarity that is in line with the implementation of CLIP and does not rely on any unknown information about the distributions of (X, Y) .

C.1.1 Proof of Lemma 8

Recall the definition of mutual information

$$I(X; Y) = D_{\text{KL}}(P_{X,Y} \parallel P_X \otimes P_Y),$$

where $P_{X,Y}$ is the joint distribution of (X, Y) and P_X, P_Y are marginal distributions. For any map f and g , we have the

$$I(X; Y) \geq I(f(X); g(Y)).$$

When f and g are one-to-one with measurable inverse maps, it holds that $I(X; Y) = I(f(X); g(Y))$.

To characterize the dependence structure between $f(X)$ and $g(Y)$, the conditional distribution $P_{f(X)|g(X)}$ is often of interest, but the estimation is usually not tractable in practice. As an alternative, consider a hypothesized conditional distribution $Q_{f(X)|g(Y),\tau}$ with density function $q_{f(X)|g(Y),\tau}$, with which we have

$$\begin{aligned} I(f(X); g(Y)) &= \mathbb{E}_P \left[\log \frac{p_{f(X),g(Y)}(U, V)}{p_{f(X)}(U)p_{g(Y)}(V)} \right] \\ &= \mathbb{E}_P \left[\log \frac{p_{f(X)|g(Y)}(U | V)q_{f(X)|g(Y),\tau}(U | V)}{p_{f(X)}(U)q_{f(X)|g(Y),\tau}(U | V)} \right] \\ &= \mathbb{E}_P \left[\log \frac{q_{f(X)|g(Y),\tau}(U | V)}{p_{f(X)}(U)} \right] + \mathbb{E}_{P_{g(Y)}} [D_{\text{KL}}(P_{f(X)|g(Y)} \parallel Q_{f(X)|g(Y),\tau})]. \end{aligned}$$

Similarly, if we have a hypothesized conditional distribution $\tilde{Q}_{g(Y)|f(X),\tau}$ with density function $\tilde{q}_{g(Y)|f(X),\tau}$, we can symmetrize the foregoing argument to obtain

$$\begin{aligned} I(f(X); g(Y)) &= \frac{1}{2} \mathbb{E}_P \left[\log \frac{q_{f(X)|g(Y),\tau}(U | V)}{p_{f(X)}(U)} \right] + \frac{1}{2} \mathbb{E}_{P_{g(Y)}} [D_{\text{KL}}(P_{f(X)|g(Y)} \parallel Q_{f(X)|g(Y),\tau})] \\ &\quad + \frac{1}{2} \mathbb{E}_P \left[\log \frac{\tilde{q}_{g(Y)|f(X),\tau}(V | U)}{p_{g(Y)}(V)} \right] + \frac{1}{2} \mathbb{E}_{P_{f(X)}} [D_{\text{KL}}(P_{g(Y)|f(X)} \parallel \tilde{Q}_{g(Y)|f(X),\tau})]. \end{aligned}$$

We consider the following families of conditional distributions:

$$\begin{aligned} \mathcal{H}_{f|g} &= \left\{ q_{f(X)|g(Y),\tau}(u | v) = p_{f(X)}(u) \cdot \frac{e^{\sigma(u,v)/\tau}}{\mathbb{E}_{P_{g(Y)}} e^{\sigma(u,V)/\tau}} \right\}, \\ \mathcal{H}_{g|f} &= \left\{ \tilde{q}_{g(Y)|f(X),\tau}(v | u) = p_{g(Y)}(v) \cdot \frac{e^{\sigma(u,v)/\tau}}{\mathbb{E}_{P_{f(X)}} e^{\sigma(U,v)/\tau}} \right\}, \end{aligned}$$

where $\sigma(U, V)$ is a similarity measure between random vectors U and V . Then, in this case, for any $q_{f(X)|g(Y),\tau}(u | v) \in \mathcal{H}_{f|g}$ and $\tilde{q}_{g(Y)|f(X),\tau}(v | u) \in \mathcal{H}_{g|f}$, one can verify that

$$\begin{aligned} \mathbb{E}_P \left[\log \frac{q_{f(X)|g(Y),\tau}(U | V)}{p_{f(X)}(U)} \right] &= \frac{1}{\tau} \mathbb{E}_P \{ \sigma(f(X), g(Y)) \} - \mathbb{E}_X \left\{ \log \mathbb{E}_{\tilde{Y}} \left[\exp \left(\frac{\sigma(f(X), g(\tilde{Y}))}{\tau} \right) \right] \right\}, \\ \mathbb{E}_P \left[\log \frac{\tilde{q}_{g(Y)|f(X),\tau}(V | U)}{p_{g(Y)}(V)} \right] &= \frac{1}{\tau} \mathbb{E}_P \{ \sigma(f(X), g(Y)) \} - \mathbb{E}_{\tilde{Y}} \left\{ \log \mathbb{E}_X \left[\exp \left(\frac{\sigma(f(X), g(\tilde{Y}))}{\tau} \right) \right] \right\}. \end{aligned}$$

In addition, if we define the joint distributions

$$Q_{f(X),g(Y),\tau} = Q_{f(X)|g(Y),\tau} \otimes P_{g(Y)} \quad \text{and} \quad \tilde{Q}_{f(X),g(Y),\tau} = \tilde{Q}_{g(Y)|f(X),\tau} \otimes P_{f(X)}, \quad (6)$$

we obtain the variational form of mutual information as follows:

$$\begin{aligned} I(f(X); g(Y)) &= -\frac{1}{2}\mathcal{L}(f, g, \tau) \\ &\quad + \frac{1}{2}D_{\text{KL}}(P_{f(X),g(Y)} \parallel Q_{f(X),g(Y),\tau}) + \frac{1}{2}D_{\text{KL}}(P_{f(X),g(Y)} \parallel \tilde{Q}_{f(X),g(Y),\tau}) \\ &=: -\frac{1}{2}\mathcal{L}(f, g, \tau) + \Delta(P; Q_{f(X),g(Y),\tau}, \tilde{Q}_{f(X),g(Y),\tau}). \end{aligned}$$

Hence, minimizing $\mathcal{L}(f, g, \tau)$ is equivalent to the following optimization problem:

$$\begin{aligned} \min_{f,g,\tau} \quad & \left\{ -I(f(X); g(Y)) + \Delta(P; Q_{f(X),g(Y),\tau}, \tilde{Q}_{f(X),g(Y),\tau}) \right\} \\ \text{subject to} \quad & dQ_{f(X)|g(Y),\tau} \in \mathcal{H}_{f|g}, \quad d\tilde{Q}_{g(Y)|f(X),\tau} \in \mathcal{H}_{g|f}. \end{aligned}$$

C.2 Properties of (approximate) minimizers

Since temperature τ is also optimized, to analyze the solution path with varying τ , for any $\varepsilon > 0$, we consider the set

$$O_{\mathcal{L},\varepsilon,\eta}(\mathcal{H}) = \left\{ (f, g) \in \mathcal{H} : \exists \tau \geq \varepsilon \text{ such that } \limsup_{M \rightarrow +\infty} (\mathcal{L}(f_M, g_M, \tau) + 2I_M^*(\mathcal{H})) \leq 2\eta \right\}. \quad (7)$$

Note that we adopt the natural order \leq on \mathbb{R} since with discretization, it always holds that $I_M^*(\mathcal{H}) < +\infty$. Recall that

$$O_{\mathcal{L},\eta}(\mathcal{H}) = \left\{ (f, g) \in \mathcal{H} : \exists \tau \geq \varepsilon(\eta) \text{ such that } \limsup_{M \rightarrow +\infty} (\mathcal{L}(f_M, g_M, \tau) + 2I_M^*(\mathcal{H})) \leq 2\eta \right\},$$

where we define $\varepsilon(\eta)$ as follows. Denote the set of nondecreasing univariate functions by \mathcal{C} and in addition, the subset

$$\mathcal{C}^* = \left\{ \omega(\cdot) \in \mathcal{C} : \bigcap_{\eta \geq 0} O_{\mathcal{L},\omega(\eta),\eta}(\mathcal{H}) \neq \emptyset, \quad \lim_{\eta \rightarrow 0+} \omega(\eta) = 0 \right\}. \quad (8)$$

The set \mathcal{C}^* is shown to be nonempty when $\mathcal{V}(\mathcal{H}) \neq \emptyset$ in Lemma 9. We define $\omega_1(\cdot) \preceq \omega_2(\cdot)$ if for any $\eta \geq 0$, it holds that $\omega_1(\eta) \leq \omega_2(\eta)$. Then, we choose $\varepsilon(\cdot)$ to be any item in \mathcal{C}^* such that

$$\{\omega \in \mathcal{C}^* : \varepsilon(\cdot) \preceq \omega(\cdot)\} = \emptyset. \quad (9)$$

Note that if there exists a global minimizer (f, g) that minimizes \mathcal{L} for any $\tau \geq 0$, we can simply define

$$\varepsilon(\eta) = \sup \left\{ \varepsilon \geq 0 : O_{\mathcal{L},\eta,\varepsilon}(\mathcal{H}) \neq \emptyset \right\}.$$

To start with, we have the following lemma.

Lemma 9. Assume $\mathcal{V}(\mathcal{H}) \neq \emptyset$. Then, it holds that

$$\bigcap_{\eta \geq 0} \mathcal{O}_{\mathcal{L}, \eta}(\mathcal{H}) \neq \emptyset.$$

In addition, $\liminf_{\eta \rightarrow 0} \varepsilon(\eta) = 0$.

See proof in Section C.2.1.

Then, we are ready to present the main result on the properties of $\cap_{\eta \geq 0} \mathcal{O}_{\mathcal{L}, \eta}(\mathcal{H})$. For a general similarity measure $\sigma(U, V)$ and any $(f, g) \in \cap_{\eta \geq 0} \mathcal{O}_{\mathcal{L}, \eta}(\mathcal{H})$, we have the following results.

Lemma 10. Assume $(f, g) \in \cap_{\eta \geq 0} \mathcal{O}_{\mathcal{L}, \eta}(\mathcal{H})$ and $m_\sigma(f, g) < \infty$. Then, the following properties hold.

- (1) **Maximal mutual information.** $(f, g) \in \mathcal{W}(\mathcal{H})$.
- (2) **Maximal similarity.** $\sigma(f(X), g(Y)) = m_\sigma(f, g)$ almost surely.
- (3) **Monotonicity in τ .** $\Delta(P; Q_{f(X), g(Y), \tau}, \tilde{Q}_{f(X), g(Y), \tau})$ is increasing in τ .

C.2.1 Proof of Lemma 9

Nonemptiness. To see the nonemptiness, it suffices to show that for any $(f^*, g^*) \in \mathcal{V}(\mathcal{H})$,

$$\begin{aligned} 0 &= \lim_{\tau \rightarrow 0+} \left\{ \limsup_{M \rightarrow +\infty} (\mathcal{L}(f_M^*, g_M^*, \tau) + 2I_M^*(\mathcal{H})) \right\} \\ &= \lim_{\tau \rightarrow 0+} \left\{ \limsup_{M \rightarrow +\infty} \left(2I_M^*(\mathcal{H}) - 2I(f_M^*(X); g_M^*(Y)) + 2\Delta(P; Q_{f_M^*(X), g_M^*(Y), \tau}, \tilde{Q}_{f_M^*(X), g_M^*(Y), \tau}) \right) \right\}. \end{aligned}$$

Without loss of generality, assume $\mathbb{E}\|f^*(X)\| = \mathbb{E}\|g^*(Y)\| = 1$. By definition, since $(f^*, g^*) \in \mathcal{V}(\mathcal{H})$, we have

$$\liminf_{M \rightarrow +\infty} (I(f_M^*(X); g_M^*(Y)) - I_M^*(\mathcal{H})) = \limsup_{M \rightarrow +\infty} (I_M^*(\mathcal{H}) - I(f_M^*(X); g_M^*(Y))) = 0,$$

which implies that, for any $\tau \geq 0$,

$$\limsup_{M \rightarrow +\infty} (\mathcal{L}(f_M^*, g_M^*, \tau) + 2I_M^*(\mathcal{H})) \leq 2 \limsup_{M \rightarrow +\infty} \Delta(P; Q_{f_M^*(X), g_M^*(Y), \tau}, \tilde{Q}_{f_M^*(X), g_M^*(Y), \tau}).$$

As $(f^*, g^*) \in \mathcal{A}(\mathcal{H})$, i.e., $f^*(X) = g^*(Y)$ almost surely, we further have $p_{f^*(X)}(u) = p_{g^*(Y)}(u)$ and

$$p_{f^*(X), g^*(Y)}(u, v) = p_{f^*(X)}(u) \mathbf{1}_{u=v},$$

which is also true after discretization, i.e., $f_M^*(X) = g_M^*(Y)$ almost surely and

$$p_{f_M^*(X), g_M^*(Y)}(u, v) = p_{f_M^*(X)}(u) \mathbf{1}_{u=v}.$$

In addition, for any $M \in \mathcal{M}$,

$$\begin{aligned}
& D_{\text{KL}}(P_{f_M^*(X), g_M^*(Y)} \parallel Q_{f_M^*(X), g_M^*(Y), \tau}) \\
&= \iint_{\mathbb{R}^d \times \mathbb{R}^d} p_{f_M^*(X), g_M^*(Y)}(u, v) \log p_{f_M^*(X), g_M^*(Y)}(u, v) \mathbf{d}u \mathbf{d}v \\
&\quad - \iint_{\mathbb{R}^d \times \mathbb{R}^d} p_{f_M^*(X), g_M^*(Y)}(u, v) \log \frac{e^{1/\tau} (p_{f_M^*(X)}(u))^2}{\int_{\mathbb{R}^d} p_{f_M^*(X)}(\tilde{v}) e^{\langle u, \tilde{v} \rangle / \tau} \mathbf{d}\tilde{v}} \mathbf{d}u \mathbf{d}v \\
&= -\frac{1}{\tau} + H(f_M^*(X)) + \int_{\mathbb{R}^d} p_{f_M^*(X)}(u) \log \left(\int_{\mathbb{R}^d} p_{f_M^*(X)}(\tilde{v}) e^{\langle u, \tilde{v} \rangle / \tau} \mathbf{d}\tilde{v} \right) \mathbf{d}u \\
&= \int_{\mathbb{R}^d} p_{f_M^*(X)}(u) \log \frac{\int_{\mathbb{R}^d} p_{f_M^*(X)}(\tilde{v}) e^{\langle u, \tilde{v} \rangle / \tau} \mathbf{d}\tilde{v}}{p_{f_M^*(X)}(u) e^{1/\tau}} \mathbf{d}u.
\end{aligned}$$

Then, by Lemma 2, we have

$$\lim_{M \rightarrow +\infty} D_{\text{KL}}(P_{f_M^*(X), g_M^*(Y)} \parallel Q_{f_M^*(X), g_M^*(Y), \tau}) = D_{\text{KL}}(P_{f^*(X), g^*(Y)} \parallel Q_{f^*(X), g^*(Y), \tau}),$$

for which, it holds that

$$\begin{aligned}
\lim_{\tau \rightarrow 0+} D_{\text{KL}}(P_{f^*(X), g^*(Y)} \parallel Q_{f^*(X), g^*(Y), \tau}) &= \lim_{\tau \rightarrow 0+} \left\{ \int_{\mathbb{R}^d} p_{f^*(X)}(u) \log \frac{\int_{\mathbb{R}^d} p_{f^*(X)}(\tilde{v}) e^{\langle u, \tilde{v} \rangle / \tau} \mathbf{d}\tilde{v}}{p_{f^*(X)}(u) e^{1/\tau}} \mathbf{d}u \right\} \\
&= \int_{\mathbb{R}^d} p_{f^*(X)}(u) \log \frac{p_{f^*(X)}(u)}{p_{f^*(X)}(u)} \mathbf{d}u = 0.
\end{aligned}$$

Hence, by the symmetry of $\Delta(P; Q_{f_M^*(X), g_M^*(Y), \tau}, \tilde{Q}_{f_M^*(X), g_M^*(Y), \tau})$ in f and g , we obtain

$$\lim_{\tau \rightarrow 0+} \left\{ \limsup_{M \rightarrow +\infty} \Delta(P; Q_{f_M^*(X), g_M^*(Y), \tau}, \tilde{Q}_{f_M^*(X), g_M^*(Y), \tau}) \right\} = 0.$$

Then, the constant function $\omega(\eta) = 0$ is in the set \mathcal{C}^* defined in (8), indicating that $\mathcal{C}^* \neq \emptyset$, thus $\cap_{\eta \geq 0} \mathcal{O}_{\mathcal{L}, \eta}(\mathcal{H}) \neq \emptyset$.

Zero limit infimum. Suppose $\liminf_{\eta \rightarrow 0} \varepsilon(\eta) = \underline{\tau} > 0$. Then, for any $(f, g) \in \mathcal{H}$, it holds that

$$\limsup_{M \rightarrow +\infty} (\mathcal{L}(f_M, g_M, \underline{\tau}) + 2I_M^*(\mathcal{H})) \leq 0.$$

In addition, as we have shown in Lemma 8, it holds that

$$\mathcal{L}(f_M, g_M, \tau) + 2I_M^*(\mathcal{H}) \geq -2I(f_M(X); g_M(Y)) + 2I_M^*(\mathcal{H}) \geq 0,$$

which further implies that

$$0 \leq \liminf_{M \rightarrow +\infty} (\mathcal{L}(f_M, g_M, \underline{\tau}) + 2I_M^*(\mathcal{H})) \leq \limsup_{M \rightarrow +\infty} (\mathcal{L}(f_M, g_M, \underline{\tau}) + 2I_M^*(\mathcal{H})) \leq 0.$$

Hence, $\lim_{M \rightarrow +\infty} (\mathcal{L}(f_M^*, g_M^*, \underline{\tau}) + 2I_M^*(\mathcal{H})) = 0$. Moreover, as

$$\mathcal{L}(f_M, g_M, \underline{\tau}) + 2I_M^*(\mathcal{H}) \geq \Delta(P; Q_{f_M(X), g_M(Y), \underline{\tau}}, \tilde{Q}_{f_M(X), g_M(Y), \underline{\tau}}) \geq 0,$$

we further obtain

$$\lim_{M \rightarrow +\infty} \Delta(P; Q_{f_M(X), g_M(Y), \underline{\tau}}, \tilde{Q}_{f_M(X), g_M(Y), \underline{\tau}}) = 0.$$

In this case, the joint distribution of $(f(X), g(Y))$ takes the form

$$p_{f(X), g(Y)}(u, v) = \frac{\exp\left(\frac{\sigma(u, v)}{\underline{\tau}}\right) p_{f(X)}(u) p_{g(Y)}(v)}{\mathbb{E}_{P_{f(X)} \otimes P_{g(Y)}} \exp\left(\frac{\sigma(f(X), g(Y))}{\underline{\tau}}\right)},$$

thus, the mutual information satisfies

$$\begin{aligned} I(f(X); g(Y)) &= \iint p_{f(X), g(Y)}(u, v) \log \frac{p_{f(X), g(Y)}(u, v)}{p_{f(X)}(u) p_{g(Y)}(v)} \mathrm{d}u \mathrm{d}v \\ &\leq \iint \frac{\sigma(u, v)}{\underline{\tau}} \cdot \frac{\exp\left(\frac{\sigma(u, v)}{\underline{\tau}}\right) p_{f(X)}(u) p_{g(Y)}(v)}{\mathbb{E}_{P_{f(X)} \otimes P_{g(Y)}} \exp\left(\frac{\sigma(f(X), g(Y))}{\underline{\tau}}\right)} \mathrm{d}u \mathrm{d}v \\ &\quad - \log \mathbb{E}_{P_{f(X)} \otimes P_{g(Y)}} \exp\left(\frac{\sigma(f(X), g(Y))}{\underline{\tau}}\right) \\ &\leq \frac{\Omega}{\underline{\tau}} < \infty. \end{aligned}$$

Hence, $\limsup_{M \rightarrow +\infty} I(f_M(X); g_M(Y)) < \infty$ for any $(f, g) \in \mathcal{H}$. Then, we obtain

$$\limsup_{M \rightarrow +\infty} I_M^*(\mathcal{H}) = \limsup_{M \rightarrow +\infty} \sup_{(f, g) \in \mathcal{H}} I(f_M(X); g_M(Y)) \leq \frac{\Omega}{\underline{\tau}} < \infty. \quad (10)$$

In addition, since $\mathcal{V}(\mathcal{H}) \neq \emptyset$, there exist (f^*, g^*) such that $f^*(X)/\mathbb{E}\|f^*(X)\| = g^*(Y)/\mathbb{E}\|g^*(Y)\|$ almost surely, thus

$$\limsup_{M \rightarrow +\infty} I_M^*(\mathcal{H}) \geq \limsup_{M \rightarrow +\infty} I(f_M^*(X); g_M^*(X)) = +\infty,$$

which draws the contradiction to (10).

C.2.2 Proof of Lemma 10 (1) and (2)

Assume $(f, g) \in \cap_{\eta \geq 0} \mathcal{O}_{\mathcal{L}, \eta}(\mathcal{H})$. There exists a decreasing sequence $\{\eta_j\}_{j \in \mathbb{N}}$ such that $\eta_j \rightarrow 0$ as $j \rightarrow +\infty$. Accordingly, there is an associated sequence $\tau_j = \varepsilon(\eta_j)$, which satisfies $\liminf_{j \rightarrow +\infty} \tau_j = 0$ as is shown in Lemma 9. By the decomposition in Lemma 8 and the definition of $\mathcal{O}_{\mathcal{L}, \eta}(\mathcal{H})$, for any $j \in \mathbb{N}$, it holds that

$$\limsup_{M \rightarrow +\infty} \left\{ I_M^*(\mathcal{H}) - I(f_M(X); g_M(Y)) + \Delta(P; Q_{f_M(X), g_M(Y), \tau_j}, \tilde{Q}_{f_M(X), g_M(Y), \tau_j}) \right\} \leq \eta_j.$$

Since $\liminf_{j \rightarrow +\infty} \tau_j = 0$, there is a convergent subsequence $\{\tau_{j_l}\}_{l \in \mathbb{N}}$ with $\lim_{l \rightarrow +\infty} \tau_{j_l} = 0$. Without loss of generality, we assume $\{\tau_j\}_{j \in \mathbb{N}}$ is convergent such that $\lim_{j \rightarrow +\infty} \tau_j = 0$.

In addition, we have, for any $M \in \mathcal{M}$ and $j \in \mathbb{N}$,

$$I_M^*(\mathcal{H}) - I(f_M(X); g_M(Y)) \geq 0, \quad \Delta(P; Q_{f_M(X), g_M(Y), \tau_j}, \tilde{Q}_{f_M(X), g_M(Y), \tau_j}) \geq 0,$$

which implies that

$$\begin{aligned} & \max \left\{ \limsup_{M \rightarrow +\infty} \{I_M^*(\mathcal{H}) - I(f_M(X); g_M(Y))\}, \limsup_{M \rightarrow +\infty} \left\{ \Delta(P; Q_{f_M(X), g_M(Y), \tau_j}, \tilde{Q}_{f_M(X), g_M(Y), \tau_j}) \right\} \right\} \\ & \leq \limsup_{M \rightarrow +\infty} \left\{ I_M^*(\mathcal{H}) - I(f_M(X); g_M(Y)) + \Delta(P; Q_{f_M(X), g_M(Y), \tau_j}, \tilde{Q}_{f_M(X), g_M(Y), \tau_j}) \right\} \leq \eta_j. \end{aligned}$$

Then, by Moore-Osgood theorem (Osgood, 1907; Graves, 2012), we can exchange the order of limit operators and obtain

$$\begin{cases} \limsup_{M \rightarrow +\infty} \Delta(P; Q_{f_M(X), g_M(Y), 0}, \tilde{Q}_{f_M(X), g_M(Y), 0}) = 0, \\ \liminf_{M \rightarrow +\infty} (I(f_M(X); g_M(Y)) - I_M^*(\mathcal{H})) = 0. \end{cases}$$

Denote $m = m_\sigma(f, g) = \text{ess sup } \sigma(f(X), g(\tilde{Y}))$, and $\mathcal{E}_m = \{(u, v) \in R(f) \times R(g) : \sigma(u, v) = m\}$, $\mathcal{A}^m(u) = \{v \in R(g) : \sigma(u, v) = m\}$, $\mathcal{B}^m(v) = \{u \in R(f) : \sigma(u, v) = m\}$. As $\varepsilon \rightarrow 0$, to ensure $\limsup_{M \rightarrow +\infty} \Delta(P^M; Q_{\tilde{\varepsilon}}^M, \tilde{Q}_{\tilde{\varepsilon}}^M) = 0$, we have

$$\begin{aligned} p_{f(X), g(Y)}(u, v) &= p_{f(X)}(u) p_{g(Y)}(v) \frac{\mathbf{1}_{\sigma(u, v) = m}}{\mathbb{E}_{g(Y)}[\mathbf{1}_{\{V: \sigma(u, V) = m\}}]} \\ &= p_{f(X)}(u) p_{g(Y)}(v) \frac{\mathbf{1}_{\sigma(u, v) = m}}{\mathbb{E}_{f(X)}[\mathbf{1}_{\{U: \sigma(U, v) = m\}}]}, \end{aligned} \tag{11}$$

which indicates that

$$\begin{aligned} \mathbb{E}_{g(Y)}[\mathbf{1}_{\{V: \sigma(u, V) = m\}}] &= \mathbb{E}_{f(X)}[\mathbf{1}_{\{U: \sigma(U, v) = m\}}] \\ &= \iint_{\mathcal{E}_m} p_{f(X)}(u) p_{g(Y)}(v) du dv := A_m. \end{aligned}$$

Here $\mathbf{1}_A$ is the indicator function with respect to the set A and if $A = \{a\}$, we define $\mathbb{E}_{f(X)}[\mathbf{1}_A] = p_{f(X)}(a)$. In this case, $\sigma(f(X), g(Y)) = m$ almost surely, which completes the proof.

C.2.3 Proof of Lemma 10 (3)

Recall the definition

$$\begin{aligned} & \Delta(P; Q_{f(X), g(Y), \tau}, \tilde{Q}_{f(X), g(Y), \tau}) \\ &= \frac{1}{2} D_{\text{KL}}(P_{f(X), g(Y)} \parallel Q_{f(X), g(Y), \tau}) + \frac{1}{2} D_{\text{KL}}(P_{f(X), g(Y)} \parallel \tilde{Q}_{f(X), g(Y), \tau}). \end{aligned}$$

It suffices to show the monotonicity of the first term in τ . Since infoNCE loss is scale-invariant with respect to both f and g , without loss of generality, we can assume $\mathbb{E}\|f(X)\| = \mathbb{E}\|g(Y)\| = 1$.

When the distribution $P_{f(X), g(Y)}$ degenerates on the support $\{\sigma(f(X), g(Y)) = m_\sigma(f, g)\}$, $P_{f(X), g(Y)}$ is not absolutely continuous with respect to $Q_{f(X), g(Y), \tau}$ and $\tilde{Q}_{f(X), g(Y), \tau}$, thus $\Delta(P; Q_{f(X), g(Y), \tau}, \tilde{Q}_{f(X), g(Y), \tau}) = +\infty$ for any $\tau > 0$ and $\Delta(P; Q_{f(X), g(Y), \tau}, \tilde{Q}_{f(X), g(Y), \tau}) = 0$ if and only if $\tau = 0$.

If the distribution $P_{f(X),g(Y)}$ is not degenerate, by the joint distribution in (11), we further have

$$\begin{aligned}
& D_{\text{KL}}(P_{f(X),g(Y)} \parallel Q_{f(X),g(Y),\tau}) \\
&= \iint_{\mathbb{R}^d \times \mathbb{R}^d} p_{f(X),g(Y)}(u, v) \log \frac{p_{f(X),g(Y)}(u, v)}{q_{f(X),g(Y),\tau}(u, v)} \mathbf{d}u \mathbf{d}v \\
&= \iint_{\mathbb{R}^d \times \mathbb{R}^d} p_{f(X),g(Y)}(u, v) \log \frac{p_{f(X),g(Y)}(u, v)}{p_{f(X)}(u)p_{g(Y)}(v)} \mathbf{d}u \mathbf{d}v \\
&\quad - \iint_{\mathbb{R}^d \times \mathbb{R}^d} p_{f(X),g(Y)}(u, v) \log \frac{e^{m/\tau}}{\int_{\mathbb{R}^d} p_{g(Y)}(\tilde{v}) e^{\sigma(u,\tilde{v})/\tau} \mathbf{d}\tilde{v}} \mathbf{d}u \mathbf{d}v.
\end{aligned}$$

Then, since the first term is free of τ , we have

$$\begin{aligned}
& \frac{\partial}{\partial \tau} D_{\text{KL}}(P_{f(X),g(Y)} \parallel Q_{f(X),g(Y),\tau}) \\
&= \frac{\partial}{\partial \tau} \left\{ - \iint_{\mathbb{R}^d \times \mathbb{R}^d} p_{f(X),g(Y)}(u, v) \log \frac{e^{m/\tau}}{\int_{\mathbb{R}^d} p_{g(Y)}(\tilde{v}) e^{\sigma(u,\tilde{v})/\tau} \mathbf{d}\tilde{v}} \mathbf{d}u \mathbf{d}v \right\} \\
&= \frac{\partial}{\partial \tau} \left\{ - \frac{m}{\tau} + \iint_{\mathbb{R}^d \times \mathbb{R}^d} p_{f(X),g(Y)}(u, v) \left[\log \int_{\mathbb{R}^d} p_{g(Y)}(\tilde{v}) e^{\sigma(u,\tilde{v})/\tau} \mathbf{d}\tilde{v} \right] \mathbf{d}u \mathbf{d}v \right\} \\
&= \frac{1}{\tau^2} \left\{ m - \iint_{\mathbb{R}^d \times \mathbb{R}^d} p_{f(X),g(Y)}(u, v) \left[\frac{\int_{\mathbb{R}^d} \sigma(u, \tilde{v}) p_{g(Y)}(\tilde{v}) e^{\sigma(u,\tilde{v})/\tau} \mathbf{d}\tilde{v}}{\int_{\mathbb{R}^d} p_{g(Y)}(\tilde{v}) e^{\sigma(u,\tilde{v})/\tau} \mathbf{d}\tilde{v}} \right] \mathbf{d}u \mathbf{d}v \right\}.
\end{aligned}$$

Since $\sigma(u, \tilde{v}) \leq m$, the derivative is nonnegative, thus

$$\frac{\partial}{\partial \tau} D_{\text{KL}}(P_{f(X),g(Y)} \parallel Q_{f(X),g(Y),\tau}) \geq 0.$$

The equality holds if and only if $\sigma(f(X), g(\tilde{Y})) = m_\sigma(f, g)$ almost surely with respect to the product distribution $P_{f(X)} \otimes P_{g(Y)}$. In this case, for any $\tau \geq 0$, the infoNCE loss $\mathcal{L}(f, g, \tau) = 0$, which contradicts the fact that $(f, g) \in \cap_{\eta \geq 0} \mathcal{O}_{\mathcal{L}, \eta}(\mathcal{H})$, thus, we have

$$\frac{\partial}{\partial \tau} D_{\text{KL}}(P_{f(X),g(Y)} \parallel Q_{f(X),g(Y),\tau}) > 0.$$

By the symmetry of $\Delta(P; Q_{f(X),g(Y),\tau}, \tilde{Q}_{f(X),g(Y),\tau})$ in f and g , we conclude that $\Delta(P; Q_{f(X),g(Y),\tau}, \tilde{Q}_{f(X),g(Y),\tau})$ is increasing in τ .

D Proof of Theorem 2

We present the proof of Theorem 2 in this section. If $\mathcal{V}(\mathcal{H}) \neq \emptyset$, we have $\mathcal{V}(\mathcal{H}) = \mathcal{V}(\mathcal{H}^{k*})$ as a result of Lemma 7 and $\cap_{\eta \geq 0} \mathcal{O}_{\mathcal{L}, \eta}(\mathcal{H}) \neq \emptyset$ as a result of Lemma 9, respectively.

In addition, Theorem 2 (1)(3)(4) are directly implied by Lemma 10, thus it suffices to prove Theorem 2 (2).

Based on the previous notations, we will prove the result with the following steps.

- **Step 1:** for any $(f, g) \in \cap_{\eta \geq 0} \mathcal{O}_{\mathcal{L}, \eta}(\mathcal{H})$, it holds that $\min\{\text{ID}(f), \text{ID}(g)\} \geq k^*$;
- **Step 2:** for any $(f, g) \in \cap_{\eta \geq 0} \mathcal{O}_{\mathcal{L}, \eta}(\mathcal{H})$, $\max\{\text{ID}(f), \text{ID}(g)\} \leq k^*$.

Combining the two steps, we conclude that for any $(f, g) \in \cap_{\eta \geq 0} \mathcal{O}_{\mathcal{L}, \eta}(\mathcal{H})$, it holds that $\text{ID}(f) = \text{ID}(g) = k^*$.

D.1 Proof of Step 1

If $\text{ID}(f) = k < k^* \leq d$, there exists a random vector $Z \in \mathcal{B}_k$ such that $f(X) = \phi(Z)$ almost surely for some injective measurable function $\phi : \mathbb{R}^k \rightarrow \mathbb{R}^d$. In addition, we have $\text{ID}(g) < d$. To see this, suppose $\text{ID}(g) = d$. Consider $(u, v) \in R(f) \times R(g)$ such that $\langle u, v \rangle = m_\sigma(f, g) \mathbb{E}\|f(X)\| \mathbb{E}\|g(Y)\|$ and there exists an open set \mathcal{B}_v satisfying $v \in \mathcal{B}_v \subseteq R(g)$. Then, consider the linear function $\zeta(z) = \langle u, z \rangle$, which is continuous in $z \in \mathcal{B}_v$. There exists $\tilde{v} \in \mathcal{B}_v \subseteq R(g)$ such that $\zeta(\tilde{v}) = \langle u, \tilde{v} \rangle > \zeta(v) = m_\sigma(f, g) \mathbb{E}\|f(X)\| \mathbb{E}\|g(Y)\|$, which draws the contradiction.

Then, there exist $F(X), G(Y) \in \mathbb{R}^k$ and injective measurable functions $\phi, \psi : \mathbb{R}^k \rightarrow \mathbb{R}^d$ such that

$$f(X) = \phi(F(X)) \quad g(Y) = \psi(G(Y)).$$

Accordingly, for any $(f^*, g^*) \in \mathcal{V}(\mathcal{H}) = \mathcal{V}(\mathcal{H}^{k^*})$, there exist $\Phi_1, \Phi_2 : \mathbb{R}^d \times \mathbb{R}^d \rightarrow \mathbb{R}$ such that

$$0 < I(\Phi_1(f(X), f^*(X)); \Phi_2(g(Y), g^*(Y)) \mid f(X)).$$

To see this, otherwise, for any $\Phi_1, \Phi_2 : \mathbb{R}^d \times \mathbb{R}^d \rightarrow \mathbb{R}$, it holds that

$$I(\Phi_1(f(X), f^*(X)); \Phi_2(g(Y), g^*(Y)) \mid f(X)) = 0,$$

which further indicates that

$$\Phi_1(f(X), f^*(X)) \perp\!\!\!\perp \Phi_2(g(Y), g^*(Y)) \mid f(X).$$

Thus, specifically, $f^*(X) \perp\!\!\!\perp g^*(Y) \mid f(X)$, which holds if and only if there exists a measurable function h such that $f^*(X) = (h \circ f)(X)$ almost surely, indicating that $\text{ID}(f^*) \leq \text{ID}(f) = k < k^*$, which draws the contradiction. By Lemma 4, we further have

$$0 \prec_{\mathcal{M}} I(\Phi_1(f(X), f^*(X)); \Phi_2(g(Y), g^*(Y)) \mid f(X)).$$

Hence, we can define

$$\tilde{F}(X) = \begin{pmatrix} F(X) \\ \mathbf{0}_{d-k-1} \\ \Phi_1(f(X), f^*(X)) \end{pmatrix} \quad \text{and} \quad \tilde{G}(Y) = \begin{pmatrix} G(Y) \\ \mathbf{0}_{d-k-1} \\ \Phi_2(g(Y), g^*(Y)) \end{pmatrix}.$$

By the Data Processing Inequality (Polyanskiy and Wu, 2014, Theorem 2.17), we have

$$\begin{aligned} -I(\tilde{F}(X); \tilde{G}(Y)) &\preceq_{\mathcal{M}} -I(F(X); \tilde{G}(Y)) \\ &\preceq_{\mathcal{M}} -I(F(X); G(Y)). \end{aligned}$$

In the first inequality, $=_{\mathcal{M}}$ holds if and only if $\tilde{G}(Y) \perp\!\!\!\perp \Phi_1(f(X), f^*(X)) \mid F(X)$, i.e.

$$\Phi_1(f(X), f^*(X)) \perp\!\!\!\perp \Phi_2(g(Y), g^*(Y)) \mid f(X),$$

drawing the contradiction to the construction of Φ , thus the first inequality is strict, i.e.

$$-I(\tilde{F}(X); \tilde{G}(Y)) \prec_{\mathcal{M}} -I(F(X); G(Y)).$$

Since ϕ and ψ are injective, we further have $-I(\tilde{F}(X); \tilde{G}(Y)) \prec_{\mathcal{M}} -I(F(X); G(Y)) =_{\mathcal{M}} -I(f(X); g(Y))$, which draws the contradiction to the fact that $(f, g) \in \mathcal{W}(\mathcal{H})$, thus $\text{ID}(f) \geq k^*$.

D.2 Proof of Step 2

As we already show that $\text{ID}(f), \text{ID}(g) \geq k^*$, let $\text{ID}(f) = k \geq k^*$. If $k^* = d$, we naturally have $k = k^*$, thus we consider the case where $k^* < d$ and there exist injective measurable functions $\phi^*, \psi^* : \mathbb{R}^{k^*} \rightarrow \mathbb{R}^d$ and $F^*(X), G^*(Y) \in \mathbb{R}^{k^*}$ such that

$$f^*(X) = \phi^*(F^*(X)) \quad g^*(Y) = \psi^*(G^*(Y)).$$

By Lemma 7, for any $(f^*, g^*) \in \mathcal{V}(\mathcal{H})$, it holds that $\text{ID}(f^*), \text{ID}(g^*) \leq k^*$ and

$$f(X) \perp\!\!\!\perp g(Y) \mid f^*(X). \quad (12)$$

Hence, we can define

$$f_*(X) = \mathbb{E}[f(X) \mid f^*(X)].$$

Then, for any $\tau > 0$, consider the infoNCE loss

$$\begin{aligned} \mathcal{L}(f, g, \tau) &= -\frac{2}{\tau} \frac{\mathbb{E}[\langle f(X), g(Y) \rangle]}{\mathbb{E}\|f(X)\| \mathbb{E}\|g(Y)\|} + \mathbb{E}_X \left\{ \log \mathbb{E}_{\tilde{Y}} \left[\exp \left(\frac{\langle f(X), g(\tilde{Y}) \rangle}{\tau \mathbb{E}\|f(X)\| \mathbb{E}\|g(\tilde{Y})\|} \right) \right] \right\} \\ &\quad + \mathbb{E}_{\tilde{Y}} \left\{ \log \mathbb{E}_X \left[\exp \left(\frac{\langle f(X), g(\tilde{Y}) \rangle}{\tau \mathbb{E}\|f(X)\| \mathbb{E}\|g(\tilde{Y})\|} \right) \right] \right\}. \end{aligned}$$

In addition, with the defined representation maps (f_*, g) , we further have

$$\begin{aligned} \mathcal{L}(f_*, g, \tau) &= -\frac{2}{\tau} \frac{\mathbb{E}[\langle f_*(X), g(Y) \rangle]}{\mathbb{E}\|f_*(X)\| \mathbb{E}\|g(Y)\|} + \mathbb{E}_X \left\{ \log \mathbb{E}_{\tilde{Y}} \left[\exp \left(\frac{\langle f_*(X), g(\tilde{Y}) \rangle}{\tau \mathbb{E}\|f_*(X)\| \mathbb{E}\|g(\tilde{Y})\|} \right) \right] \right\} \\ &\quad + \mathbb{E}_{\tilde{Y}} \left\{ \log \mathbb{E}_X \left[\exp \left(\frac{\langle f_*(X), g(\tilde{Y}) \rangle}{\tau \mathbb{E}\|f_*(X)\| \mathbb{E}\|g(\tilde{Y})\|} \right) \right] \right\}, \end{aligned}$$

where, by Jensen's inequality, $\|f_*(X)\| = \|\mathbb{E}[f(X) \mid f^*(X)]\| \leq \mathbb{E}[\|f(X)\| \mid f^*(X)]$ almost surely.

We note that, according to Lemma 10, it holds that

$$\langle f(X), g(Y) \rangle = m_{\sigma}(f, g) \cdot \mathbb{E}\|f(X)\| \mathbb{E}\|g(Y)\| \quad \text{almost surely.}$$

In addition, by the conditional independence (12), we further obtain

$$\mathbb{E} \{ \langle \mathbb{E}[f(X) \mid f^*(X)], g(Y) \rangle \} = \mathbb{E} \{ \mathbb{E}[\langle f(X), g(Y) \rangle \mid f^*(X)] \} = m_{\sigma}(f, g) \cdot \mathbb{E}\|f(X)\| \mathbb{E}\|g(Y)\|$$

almost surely and, in the meantime,

$$\begin{aligned} & \mathbb{E}_X \left\{ \log \mathbb{E}_{\tilde{Y}} \left[\exp \left(\frac{\langle f(X), g(\tilde{Y}) \rangle}{\tau \mathbb{E} \|f(X)\| \mathbb{E} \|g(\tilde{Y})\|} \right) \right] \right\} \\ &= \mathbb{E}_{f^*(X)} \left\{ \mathbb{E} \left[\log \mathbb{E}_{g(\tilde{Y})} \left\{ \exp \left(\frac{\langle f(X), g(\tilde{Y}) \rangle}{\tau \mathbb{E} \|f(X)\| \mathbb{E} \|g(\tilde{Y})\|} \right) \right\} \mid f^*(X) \right] \right\}. \end{aligned}$$

Since $\log \mathbb{E}_U \exp(x^\top U)$ is convex in x , by Jensen's inequality, we obtain

$$\begin{aligned} & \mathbb{E}_X \left\{ \log \mathbb{E}_{\tilde{Y}} \left[\exp \left(\frac{\langle f(X), g(\tilde{Y}) \rangle}{\tau \mathbb{E} \|f(X)\| \mathbb{E} \|g(\tilde{Y})\|} \right) \right] \right\} \\ & \geq \mathbb{E}_{f^*(X)} \left\{ \log \mathbb{E}_{g(\tilde{Y})} \left\{ \exp \left(\frac{\langle \mathbb{E}[f(X) \mid f^*(X)], g(\tilde{Y}) \rangle}{\tau \mathbb{E} \|f(X)\| \mathbb{E} \|g(\tilde{Y})\|} \right) \right\} \right\} \\ &= \mathbb{E}_X \left\{ \log \mathbb{E}_{\tilde{Y}} \left[\exp \left(\frac{\langle f_*(X), g(\tilde{Y}) \rangle}{\tau \mathbb{E} \|f(X)\| \mathbb{E} \|g(\tilde{Y})\|} \right) \right] \right\}. \end{aligned}$$

In addition, since $\exp(x^\top U)$ is convex in x , we also obtain

$$\mathbb{E}_X \left[\exp \left(\frac{\langle f(X), g(\tilde{Y}) \rangle}{\tau \mathbb{E} \|f(X)\| \mathbb{E} \|g(\tilde{Y})\|} \right) \right] \geq \mathbb{E}_{f^*(X)} \left[\exp \left(\frac{\langle \mathbb{E}[f(X) \mid f^*(X)], g(\tilde{Y}) \rangle}{\tau \mathbb{E} \|f(X)\| \mathbb{E} \|g(\tilde{Y})\|} \right) \right]$$

Combining the pieces above, if we define

$$\tilde{\tau} = \tau \cdot \frac{\mathbb{E} \|f_*(X)\|}{\mathbb{E} \|f(X)\|} \leq \tau,$$

it holds that

$$\mathcal{L}(f_*, g, \tau) \leq \mathcal{L}(f, g, \tilde{\tau}),$$

where the equality holds if and only if $f(X)$ can be expressed as a measurable function of $f^*(X)$ almost surely. Thus, if $f(X)$ cannot be expressed as functions of $f^*(X)$, we have

$$\mathcal{L}(f, g, \tilde{\tau}) > \mathcal{L}(f_*, g, \tau). \quad (13)$$

Then, according to Lemma 10 (3), since $\tau \geq \tilde{\tau} \geq 0$, it holds that

$$\Delta(f, g, \tau) \geq \Delta(f, g, \tilde{\tau}),$$

which, by Lemma 2 further implies that

$$\limsup_{M \rightarrow +\infty} (\mathcal{L}(f_M, g_M, \tau) + 2I_M^*(\mathcal{H})) \geq \limsup_{M \rightarrow +\infty} (\mathcal{L}(f_M, g_M, \tilde{\tau}) + 2I_M^*(\mathcal{H})).$$

According to (13) and Lemma 5, we further obtain

$$\begin{aligned} \liminf_{M \rightarrow +\infty} (\mathcal{L}(f_M, g_M, \tilde{\tau}) - \mathcal{L}((f_*)_M, g_M, \tau)) & \geq \liminf_{M \rightarrow +\infty} \mathcal{L}(f_M, g_M, \tilde{\tau}) - \limsup_{M \rightarrow +\infty} \mathcal{L}((f_*)_M, g_M, \tau) \\ &= \lim_{M \rightarrow +\infty} \mathcal{L}(f_M, g_M, \tilde{\tau}) - \lim_{M \rightarrow +\infty} \mathcal{L}((f_*)_M, g_M, \tau) > 0. \end{aligned}$$

Hence, it holds that

$$\begin{aligned}
\limsup_{M \rightarrow +\infty} (\mathcal{L}(f_M, g_M, \tau) + 2I_M^*(\mathcal{H})) &\geq \limsup_{M \rightarrow +\infty} (\mathcal{L}(f_M, g_M, \tilde{\tau}) + 2I_M^*(\mathcal{H})) \\
&\geq \limsup_{M \rightarrow +\infty} (\mathcal{L}((f_*)_M, g_M, \tau) + 2I_M^*(\mathcal{H})) \\
&\quad + \liminf_{M \rightarrow +\infty} (\mathcal{L}(f_M, g_M, \tilde{\tau}) - \mathcal{L}((f_*)_M, g_M, \tau)) \\
&> \limsup_{M \rightarrow +\infty} (\mathcal{L}((f_*)_M, g_M, \tau) + 2I_M^*(\mathcal{H})).
\end{aligned}$$

Particularly, for any $\eta > 0$, with $\tau = \varepsilon(\eta)$, it holds that

$$\begin{aligned}
\limsup_{M \rightarrow +\infty} (\mathcal{L}(f_M, g_M, \varepsilon(\eta)) + 2I_M^*(\mathcal{H})) &> \limsup_{M \rightarrow +\infty} (\mathcal{L}((f_*)_M, g_M, \varepsilon(\eta)) + 2I_M^*(\mathcal{H})) \\
&\geq 2\eta, \quad \text{for all } \eta > 0.
\end{aligned}$$

Then, by the definition of $\mathcal{O}_{\mathcal{L}, \eta}(\mathcal{H})$, we can conclude that $(f, g) \notin \mathcal{O}_{\mathcal{L}, \eta}(\mathcal{H})$, which draws the contradiction. Hence, there exist measurable functions \tilde{h} and $\tilde{\ell}$ such that

$$f(X) = (h \circ f^*)(X) \quad g(Y) = (\ell \circ g^*)(Y) \quad \text{almost surely.}$$

By Lemma 6, it holds that $\text{ID}(f), \text{ID}(g) \leq k^*$, and combining with the result in Step 1, we obtain $\text{ID}(f) = \text{ID}(g) = k^*$, which concludes the proof.

E Extensions and additional theoretical results

E.1 Connection with sufficient dimension reduction

Sufficient dimension reduction (SDR) (Li, 1991; Cook, 1996; Cook and Li, 2002) is an important topic in statistics and machine learning, in which, the goal is to find a low-dimensional representation $f(X)$ such that $f(X)$ is sufficient for the conditional distribution of $Y \mid X$ in the sense that $Y \perp\!\!\!\perp X \mid f(X)$. In the following proposition, we will show that the representations learned by CLIP are also sufficient if $\mathcal{V}(\mathcal{H}) \neq \emptyset$. To simplify notation, we focus on the case where $X, Y \in \mathbb{R}^d$. Extensions to a more general setting, where $X \in \mathbb{R}^{d_1}$ and $Y \in \mathbb{R}^{d_2}$, are provided in Appendix E.1.2. Here we denote $\text{id} : \mathbb{R}^d \rightarrow \mathbb{R}^d$ as the identical map and $X_M = \text{id}_M(X)$. Then, we have the following result.

Proposition 2. *Assume $\mathcal{V}(\mathcal{H}) \neq \emptyset$ and there exists $(f, g) \in \mathcal{H}$ such that $\liminf_{M \rightarrow +\infty} (I(f_M(X); g_M(Y)) - I(X_M; Y_M)) = 0$. For any $(f^*, g^*) \in \mathcal{V}(\mathcal{H}^{k^*})$, the dimension reductions $f^*(X)$ and $g^*(Y)$ are sufficient, i.e. $Y \perp\!\!\!\perp X \mid f^*(X)$ and $Y \perp\!\!\!\perp X \mid g^*(Y)$.*

We note that compared with Theorem 2, Proposition 2 has an additional condition that there exists $(f, g) \in \mathcal{H}$ such that $\liminf_{M \rightarrow +\infty} (I(f_M(X); g_M(Y)) - I(X_M; Y_M)) = 0$. One specific example that satisfies this condition is the scenario where we set $f^*(X) = (h_1(X), \dots, h_k(X))$ almost surely such that $Y \perp\!\!\!\perp X \mid (h_1(X), \dots, h_k(X))$, which is commonly considered in the literature of (nonlinear) SDR (Fukumizu et al., 2004, 2009; Li et al., 2011; Chen et al., 2024) and the tuple of nonlinear functions can be further extended to σ -field (Li and Song, 2017; Chen et al., 2024).

E.1.1 Proof of Proposition 2

We prove by showing that $Y \perp\!\!\!\perp X \mid f^*(X)$. By the assumption that there exists $(\tilde{f}, \tilde{g}) \in \mathcal{H}$ such that $I(Y; X) =_{\mathcal{M}} I(\tilde{f}(X); \tilde{g}(Y))$ and the definition of $\mathcal{V}(\mathcal{H}^{k*})$, it holds that $I(Y; X) =_{\mathcal{M}} I(f^*(X); g^*(Y))$ for all $(f^*, g^*) \in \mathcal{V}(\mathcal{H}^{k*})$. Then, by property of mutual information (Polyanskiy and Wu (2014) Theorem 2.3), we have

$$I(g^*(Y); f^*(X)) \preceq_{\mathcal{M}} I(Y; f^*(X)) \preceq_{\mathcal{M}} I(Y; X) =_{\mathcal{M}} I(g^*(Y); f^*(X)),$$

which implies that

$$I(Y; f^*(X)) =_{\mathcal{M}} I(Y; X). \quad (14)$$

In addition, combining (14) with the Kolmogorov identity of mutual information (Polyanskiy and Wu (2014) Theorem 2.5 (2)) that

$$I(Y; X) =_{\mathcal{M}} I(Y; X, f^*(X)) =_{\mathcal{M}} I(Y; f^*(X)) + I(Y; X \mid f^*(X)),$$

we further obtain $I(Y; X \mid f^*(X)) =_{\mathcal{M}} 0$. According to the property of the conditional mutual information (Polyanskiy and Wu (2014) Theorem 2.5 (1)), $I(Y; X \mid f^*(X)) =_{\mathcal{M}} 0$ if and only if $(X_M, f_M^*(X), Y_M)$ forms a Markov chain, i.e. $Y_M \perp\!\!\!\perp X_M \mid f_M^*(X)$ for all $M \in \mathcal{M}$, which, by continuity of X , Y , and $f^*(X)$, further indicates that $Y \perp\!\!\!\perp X \mid f^*(X)$.

E.1.2 Extension of Proposition 2

We then turn to a general case where $X \in \tilde{\mathcal{B}}_{d_1}$ and $Y \in \tilde{\mathcal{B}}_{d_2}$, where $\tilde{\mathcal{B}}_{d_1}$ and $\tilde{\mathcal{B}}_{d_2}$ are bounded sets in \mathbb{R}^{d_1} and \mathbb{R}^{d_2} , respectively. If $\mathcal{V}(\mathcal{H}) \neq \emptyset$, we fix a pair $(f^*, g^*) \in \mathcal{V}(\mathcal{H}^{k*})$. Consider discretizations $\mathcal{D}_M = \{D_{M,i}\}_{i \in [M]}$ and $\mathcal{E}_M = \{E_{M,i}\}_{i \in [M]}$ of $\tilde{\mathcal{B}}_{d_1}$ and $\tilde{\mathcal{B}}_{d_2}$, respectively, where $D_{M,i}$ is the preimage of $c_{M,i}$ under f^* and $E_{M,i}$ is the preimage of $c_{M,i}$ under g^* . Denote representatives in $D_{M,i}$ and $E_{M,i}$ by $x_{M,i}$ and $y_{M,i}$, respectively. In addition, we assume \mathcal{D}_M and \mathcal{E}_M are nested discretizations and as $M \rightarrow +\infty$, it holds that

$$\lim_{M \rightarrow +\infty} \max_{i \in [M]} \text{diam}(D_{M,i}) = 0, \quad \lim_{M \rightarrow +\infty} \max_{i \in [M]} \text{diam}(E_{M,i}) = 0.$$

Similar to notations for $\tilde{\mathcal{B}}_d$ before, we write X_M and Y_M to denote discretized random vectors where

$$\mathbb{P}(X_M = x_{M,i}) = \mathbb{P}(X \in D_{M,i}) \quad \text{and} \quad \mathbb{P}(Y_M = y_{M,i}) = \mathbb{P}(Y \in E_{M,i}).$$

Then, we define a new partial order $\preceq_{\mathcal{M}}^*$ as follows. For any random vectors $X \in \mathbb{R}^{d_1}$, $Y \in \mathbb{R}^{d_2}$, U supported on $\tilde{\mathcal{B}}_d$, and functionals F, G of random vectors, we define the order $\preceq_{\mathcal{M}}^*$ associated with (f^*, g^*) such that

$$F(X, Y) \preceq_{\mathcal{M}}^* G(U) \iff \limsup_{M \rightarrow +\infty} \{F(X_M, Y_M) - G(U_M)\} \leq 0,$$

and moreover, the inequality is strict, i.e. $F(X, Y) \prec_{\mathcal{M}}^* G(U)$, if and only if

$$\limsup_{M \rightarrow +\infty} \left\{ F(X_M, Y_M) \preceq_{\mathcal{M}}^* G(U_M) \right\} < 0.$$

We also write $F(X, Y) \stackrel{*}{=}_{\mathcal{M}} G(U)$ if $\lim_{M \rightarrow +\infty} \{F(X_M, Y_M) - G(U_M)\} = 0$. Then, we state the extension of Proposition 2 as follows.

Proposition 3. Suppose $\mathcal{V}(\mathcal{H}) \neq \emptyset$. Assume there exists $(f, g) \in \mathcal{H}$ such that $I(X; Y) \stackrel{*}{=}_{\mathcal{M}} I(f(X); g(Y))$ with $\stackrel{*}{=}_{\mathcal{M}}$ associated with $(f^*, g^*) \in \mathcal{V}(\mathcal{H}^{k^*})$. Then, the dimension reductions $f^*(X)$ and $g^*(Y)$ are sufficient, i.e.

$$Y \perp\!\!\!\perp X \mid f^*(X) \quad \text{and} \quad Y \perp\!\!\!\perp X \mid g^*(Y).$$

Proof of Proposition 3. Similar with the proof of Proposition 2, for any $(f^*, g^*) \in \mathcal{V}(\mathcal{H}^{k^*})$, it holds that

$$I(g^*(Y); f^*(X)) \stackrel{*}{\preceq}_{\mathcal{M}} I(Y; f^*(X)) \stackrel{*}{\preceq}_{\mathcal{M}} I(Y; X).$$

In addition, by assumption, there exists $(\tilde{f}, \tilde{g}) \in \mathcal{H}$ such that

$$I(Y; X) \stackrel{*}{=}_{\mathcal{M}} I(\tilde{f}(X); \tilde{g}(Y)) \stackrel{*}{\preceq}_{\mathcal{M}} I(g^*(Y); f^*(X)).$$

Combining results above, we obtain

$$I(Y; X) \stackrel{*}{=}_{\mathcal{M}} I(g^*(Y); f^*(X)).$$

In addition, by the Kolmogorov identity of mutual information (Polyanskiy and Wu (2014) Theorem 2.5 (2)), we obtain

$$I(Y; X) \stackrel{*}{=}_{\mathcal{M}} I(Y; X, f^*(X)) \stackrel{*}{=}_{\mathcal{M}} I(Y; f^*(X)) + I(Y; X \mid f^*(X)),$$

which implies that $I(Y; X \mid f^*(X)) \stackrel{*}{=}_{\mathcal{M}} 0$. According to the property of the conditional mutual information (Polyanskiy and Wu (2014) Theorem 2.5 (1)), $I(Y; X \mid f^*(X)) \stackrel{*}{=}_{\mathcal{M}} 0$ if and only if $(X_M, f_M^*(X), Y_M)$ forms a Markov chain, i.e. $Y_M \perp\!\!\!\perp X_M \mid f_M^*(X)$ for all $M \in \mathcal{M}$, which, by continuity of X , Y , and $f^*(X)$, further indicates that $Y \perp\!\!\!\perp X \mid f^*(X)$. \square

E.2 Alignment and uniformity with correctly specified dimension

To begin with, recall that for any $(f, g) \in \mathcal{A}(\mathcal{H})$, it holds that $f(X)/\mathbb{E}\|f(X)\|, g(Y)/\mathbb{E}\|g(Y)\| \in \mathcal{S}^{d-1}$. Then, we define the set of uniformly distributed representations by

$$\mathcal{U}_p(\mathcal{H}') = \{(f, g) \in \mathcal{H}' : f(X)/\mathbb{E}\|f(X)\|, g(Y)/\mathbb{E}\|g(Y)\| \sim \text{Unif}(\mathcal{S}^{p-1})\}.$$

Note that for any representation map $f \in \mathcal{H}'$ with $\text{ID}(f) = k$, if the function class is sufficiently expressive, the linear dimension of $R(f)$ can exceed k , then recalling the definition of $\mathcal{A}(\mathcal{H}^k)$ and $\mathcal{U}_p(\mathcal{H}^k)$, we define

$$D(k, \mathcal{H}) = \max \left\{ p \in [d] : \mathcal{A}(\mathcal{H}^k) \cap \mathcal{U}_p(\mathcal{H}^k) \neq \emptyset \right\}.$$

Specifically, write $d^* = D(k^*, \mathcal{H})$. Then, we define a subset of \mathcal{H} by $\mathcal{H}^* = \mathcal{H}_X^* \times \mathcal{H}_Y^*$ with

$$\begin{aligned} \mathcal{H}_X^* &= \left\{ f_{\mathcal{S}^{d^*-1}} : f \in \mathcal{H}_X, f(X)/\mathbb{E}\|f(X)\| \in \mathcal{S}^{d^*-1} \right\}, \\ \mathcal{H}_Y^* &= \left\{ g_{\mathcal{S}^{d^*-1}} : g \in \mathcal{H}_Y, g(Y)/\mathbb{E}\|g(Y)\| \in \mathcal{S}^{d^*-1} \right\}. \end{aligned}$$

We further denote $\mathcal{U}(\mathcal{H}^*) = \{(f, g) \in \mathcal{H}^* : f(X)/\mathbb{E}\|f(X)\|, g(Y)/\mathbb{E}\|g(Y)\| \sim \text{Unif}(\mathcal{S}^{d^*-1})\}$.

Then, by specifying the output dimension $d = d^*$, we have the following result.

Theorem 3. *With the function class $\mathcal{H} = \mathcal{H}^*$ and output dimension $d = d^* = D(k^*, \mathcal{H})$, it holds that*

$$\bigcap_{\eta \geq 0} \mathcal{O}_{\mathcal{L}, \eta}(\mathcal{H}^*) = \mathcal{V}(\mathcal{H}^*) \cap \mathcal{U}(\mathcal{H}^*).$$

Particularly, for any $(f^, g^*) \in \mathcal{V}(\mathcal{H}^*) \cap \mathcal{U}(\mathcal{H}^*)$, the tuple $(f^*, g^*, 0^+)$ is a minimizer of $\mathcal{L}(f, g, \tau)$.*

E.2.1 Proof of Theorem 3

By (Wang and Isola, 2020, Theorem 1 (2)), if we define $\tilde{f}(X) = f(X)/\mathbb{E}\|f(X)\|$ and $\tilde{g}(Y) = g(Y)/\mathbb{E}\|g(Y)\|$, then (\tilde{f}, \tilde{g}) is the global minimizer of \mathcal{L} in \mathcal{H}^* for any given $\tau > 0$. Then, based on the definition of $\mathcal{O}_\eta(\mathcal{H})$, it holds that

$$\mathcal{A}(\mathcal{H}^*) \cap \mathcal{U}(\mathcal{H}^*) = \bigcap_{\eta \geq 0} \mathcal{O}_{\mathcal{L}, \eta}(\mathcal{H}^*).$$

In addition, with the choice of \mathcal{H}^* , the uniformly distributed representation on \mathcal{S}^{d^*-1} maximizes the entropy. Hence, for any $(f, g) \in \mathcal{A}(\mathcal{H}^*) \cap \mathcal{U}(\mathcal{H}^*)$, we also have $(f, g) \in \mathcal{W}(\mathcal{H}^*)$, thus $\mathcal{A}(\mathcal{H}^*) \cap \mathcal{U}(\mathcal{H}^*) = \mathcal{A}(\mathcal{H}^*) \cap \mathcal{U}(\mathcal{H}^*) \cap \mathcal{W}(\mathcal{H}^*) = \mathcal{V}(\mathcal{H}^*) \cap \mathcal{U}(\mathcal{H}^*)$, which completes the proof.

F Proof of preliminary results in Section A.2

F.1 Proof of Lemma 1

We adapt the proof in (Cover, 1999, Theorem 8.3.1). The entropy of U_M can be written as

$$\begin{aligned} H(U_M) &= - \sum_{i \in [M]} p_i \log p_i \\ &= - \sum_{i \in [M]} \left(\int_{c_{M,i}} p(u) \mathrm{d}u \right) \log \left(\int_{c_{M,i}} p(u) \mathrm{d}u \right) \\ &= - \sum_{i \in [M]} [p(z_{M,i}) \log p(z_{M,i})] \Delta_M - \log \Delta_M + o(1). \end{aligned}$$

Hence, it holds that

$$\lim_{M \rightarrow +\infty} (H(U_M) + \log \Delta_M) = \tilde{H}(U).$$

F.2 Proof of Lemma 3

We note that

$$H(\phi(U_M, V_M) \mid U_M) = H(\phi(U_M, V_M), U_M) - H(U_M),$$

for which, we already see in Lemma 1 that

$$\lim_{M \rightarrow +\infty} (H(U_M) + \log \Delta_M) = \tilde{H}(U).$$

Denoting $W = \phi(U, V)$, $\zeta = \Phi(U, V) = (\phi(U, V), U)$, $w_{M,ij} = \phi(z_{M,i}, z_{M,j})$, and $\zeta_{M,ij} = (w_{M,ij}, z_{M,i})$. In addition, we write

$$q_{ij} = \mathbb{P}(U \in c_{M,i}, V \in c_{M,j}), \quad q_{ij}^\Phi = \mathbb{P}(\zeta \in \Phi(c_{M,i} \times c_{M,j})),$$

and $\Delta^\phi(z_{M,i}, z_{M,j})$ as the Lebesgue measure of $\phi(c_{M,i}, c_{M,j})$, Δ_M as the Lebesgue measure of $c_{M,i}$. Define $q^\Phi(w, u)$ as the joint density of $\Phi(U, V) = (\phi(U, V), U)$.

The joint entropy takes the form

$$\begin{aligned} & H(\phi(U_M, V_M), U_M) \\ &= - \sum_{i,j \in [M]} q_{ij}^\Phi \log q_{ij}^\Phi \\ &= - \sum_{i,j \in [M]} q^\Phi(w_{M,ij}, z_{M,i}) \Delta_M^\phi(z_{M,i}, z_{M,j}) \Delta_M \\ &\quad \times \log \left(q^\Phi(w_{M,ij}, z_{M,i}) \Delta_M^\phi(z_{M,i}, z_{M,j}) \Delta_M \right) + o(1) \\ &= - \sum_{i,j \in [M]} q^\Phi(w_{M,ij}, z_{M,i}) \Delta_M^\phi(z_{M,i}, z_{M,j}) \Delta_M \log \left(q^\Phi(w_{M,ij}, z_{M,i}) \right) \\ &\quad - \sum_{i,j \in [M]} q^\Phi(w_{M,ij}, z_{M,i}) \Delta_M^\phi(z_{M,i}, z_{M,j}) \Delta_M \log \left(\Delta_M^\phi(z_{M,i}, z_{M,j}) \Delta_M \right) + o(1) \\ &= - \sum_{i,j \in [M]} q^\Phi(w_{M,ij}, z_{M,i}) \Delta_M^\phi(z_{M,i}, z_{M,j}) \Delta_M \log \left(q^\Phi(w_{M,ij}, z_{M,i}) \right) \\ &\quad - \sum_{i,j \in [M]} q^\Phi(w_{M,ij}, z_{M,i}) \Delta_M^\phi(z_{M,i}, z_{M,j}) \Delta_M \log \Delta_M^\phi(z_{M,i}, z_{M,j}) \\ &\quad - \log \Delta_M + o(1). \end{aligned}$$

Then, by the results in Lemma 1, we obtain

$$\begin{aligned} & H(\phi(U_M, V_M), U_M) - H(U_M) \\ &= - \underbrace{\sum_{i,j \in [M]} q^\Phi(w_{M,ij}, z_{M,i}) \Delta_M^\phi(z_{M,i}, z_{M,j}) \Delta_M \log \left(q^\Phi(w_{M,ij}, z_{M,i}) \right)}_{(a)} \\ &\quad + \underbrace{\sum_{i \in [M]} [p(z_{M,i}) \Delta_M \log p(z_{M,i})]}_{(b)} \\ &\quad - \sum_{i,j \in [M]} q^\Phi(w_{M,ij}, z_{M,i}) \Delta_M^\phi(z_{M,i}, z_{M,j}) \Delta_M \log \Delta_M^\phi(z_{M,i}, z_{M,j}) + o(1), \end{aligned}$$

where, as $M \rightarrow +\infty$ and $\text{diam}(c_{M,i}) \rightarrow 0$, we have

$$\begin{cases} (a) \rightarrow -\tilde{H}(\phi(U, V), U), \\ (b) \rightarrow -\tilde{H}(U). \end{cases}$$

In addition, as $\Delta_M^\phi(z_{M,i}, z_{M,j}) < 1$,

$$\limsup_{M \rightarrow +\infty} \sum_{i,j \in [M]} q^\Phi(w_{M,ij}, z_{M,i}) \Delta_M^\phi(z_{M,i}, z_{M,j}) \Delta_M \log \Delta_M^\phi(z_{M,i}, z_{M,j}) < 0$$

Hence, we obtain

$$\begin{aligned} & \liminf_{M \rightarrow +\infty} \left(H(\phi(U_M, V_M), U_M) - H(U_M) \right) \\ & \geq \tilde{H}(\phi(U, V), U) - \tilde{H}(U) \\ & \quad - \limsup_{M \rightarrow +\infty} \sum_{i,j \in [M]} q^\Phi(w_{M,ij}, z_{M,i}) \Delta_M^\phi(z_{M,i}, z_{M,j}) \Delta_M \log \Delta_M^\phi(z_{M,i}, z_{M,j}) \\ & > \tilde{H}(\phi(U, V), U) - \tilde{H}(U) = \tilde{H}(\phi(U, V) \mid U) > 0. \end{aligned}$$

F.3 Proof of Lemma 4

Denoting $R = \phi(U, V)$, $W = \psi(U, V)$, and $r_{M,ij} = \phi(z_{M,i}, z_{M,j})$, $w_{M,ij} = \psi(z_{M,i}, z_{M,j})$, we note that

$$I(\phi(U, V); \psi(U, V)) = \iint p_{R,W}(z, w) \frac{p_{R,W}(r, w)}{p_R(r)p_W(w)} \mathrm{d}z \mathrm{d}w.$$

Denote $\Phi(U, V) = (\phi(U, V), \psi(U, V))$ and $q_{ij}^\phi = \mathbb{P}(\phi(U, V) \in \phi(c_{M,i} \times c_{M,j}))$, $q_{ij}^\psi = \mathbb{P}(\psi(U, V) \in \psi(c_{M,i} \times c_{M,j}))$, $q_{ij}^\Phi = \mathbb{P}(\Phi(U, V) \in \Phi(c_{M,i} \times c_{M,j}))$. In addition, denote $\Delta_M^\Phi(r_{M,ij}, w_{M,ij})$ as the Lebesgue measure of $\Phi(c_{M,i} \times c_{M,j})$, $\Delta_M^\phi(r_{M,ij}, w_{M,ij})$ as the Lebesgue measure of $\phi(c_{M,i} \times c_{M,j})$, and $\Delta_M^\psi(r_{M,ij}, w_{M,ij})$ as the Lebesgue measure of $\psi(c_{M,i} \times c_{M,j})$. Then, for the discretized mutual information, we have

$$\begin{aligned} & I(\phi(U_M, V_M); \psi(U_M, V_M)) \\ & = \sum_{i,j \in [M]} p_{ij}^\Phi \Delta_M^\Phi(r_{M,ij}, w_{M,ij}) \log \frac{p_{ij}^\Phi \Delta_M^\Phi(r_{M,ij}, w_{M,ij})}{p_{ij}^\phi p_{ij}^\psi \Delta_M^\phi(r_{M,ij}) \Delta_M^\psi(w_{M,ij})} + o(1). \end{aligned} \tag{15}$$

Since $\Delta_M^{\phi,\psi}(r_{M,i}, w_{M,j}) = \Delta_M^\phi(r_{M,i}) \Delta_M^\psi(w_{M,j}) + o(1)$, (15) can be further written as

$$\begin{aligned} & I(\phi(U_M, V_M); \psi(U_M, V_M)) \\ & = \sum_{i,j \in [M]} p_{ij}^\Phi \Delta_M^\Phi(r_{M,ij}, w_{M,ij}) \log \frac{p_{ij}^\Phi}{p_{ij}^\phi p_{ij}^\psi} + o(1) \\ & = \underbrace{\sum_{i,j \in [M]} (p_{ij}^\Phi \log p_{ij}^\Phi) \Delta_M^\phi(r_{M,ij}) \Delta_M^\psi(w_{M,ij})}_{(a)} \\ & \quad - \underbrace{\sum_{i,j \in [M]} \left(p_{ij}^\Phi \log (p_{ij}^\phi p_{ij}^\psi) \right) \Delta_M^\phi(r_{M,ij}) \Delta_M^\psi(w_{M,ij})}_{(b)} + o(1). \end{aligned}$$

As $M \rightarrow +\infty$ and $\max_{i \in [M]} \text{diam}(c_{M,i}) \rightarrow 0$, it holds that

$$\begin{aligned} \text{(a)} &\rightarrow -\tilde{H}(R, W), \\ \text{(b)} &\rightarrow -H_C(P_{R,W}, P_R \otimes P_W), \end{aligned}$$

where $H_C(P, Q)$ denotes the cross-entropy of Q relative to P . Hence, as $M \rightarrow +\infty$ and $\max_{i \in [M]} \text{diam}(c_{M,i}) \rightarrow 0$,

$$\text{(a)} - \text{(b)} \rightarrow D_{\text{KL}}(P_{R,W} \parallel P_R \otimes P_W) = I(R; W).$$

F.4 Proof of Lemma 5

Since infoNCE loss is scale-invariant with respect to both f and g , without loss of generality, we assume $\mathbb{E}\|f(X)\| = \mathbb{E}\|g(Y)\| = 1$. For any fineness $M \in \mathcal{M} \subseteq \mathbb{N}$, recall the infoNCE loss

$$\begin{aligned} \mathcal{L}(f_M, g_M, \tau) &= -\frac{2}{\tau} \mathbb{E} \{ \langle f_M(X), g_M(Y) \rangle \} \\ &\quad + \mathbb{E}_X \left\{ \log \mathbb{E}_{\tilde{Y}} \left[\exp \left(\frac{\langle f_M(X), g_M(\tilde{Y}) \rangle}{\tau} \right) \right] \right\} \\ &\quad + \mathbb{E}_{\tilde{Y}} \left\{ \log \mathbb{E}_X \left[\exp \left(\frac{\langle f_M(X), g_M(\tilde{Y}) \rangle}{\tau} \right) \right] \right\}. \end{aligned}$$

Similar to the proof of (Wang and Isola, 2020, Theorem 1), we have

$$\lim_{M \rightarrow +\infty} \mathbb{E} \{ \langle f_M(X), g_M(Y) \rangle \} = \mathbb{E} \{ \langle f(X), g(Y) \rangle \},$$

and, by the boundedness of $\exp(\langle f(X), g(\tilde{Y}) \rangle) \in [0, e^\Omega]$ and the dominated convergence theorem,

$$\begin{aligned} &\lim_{M \rightarrow +\infty} \mathbb{E}_X \left\{ \log \mathbb{E}_{\tilde{Y}} \left[\exp \left(\frac{\langle f_M(X), g_M(\tilde{Y}) \rangle}{\tau} \right) \right] \right\} \\ &= \lim_{M \rightarrow +\infty} \mathbb{E}_X \left\{ \log \mathbb{E}_{\tilde{Y}} \left[\exp \left(\frac{\langle f(X), g_M(\tilde{Y}) \rangle}{\tau} \right) \right] \right\} \\ &= \mathbb{E}_X \left\{ \log \mathbb{E}_{\tilde{Y}} \left[\exp \left(\frac{\langle f(X), g(\tilde{Y}) \rangle}{\tau} \right) \right] \right\}. \end{aligned}$$

Hence, it holds that

$$\lim_{M \rightarrow +\infty} \mathcal{L}(f_M, g_M, \tau) = \mathcal{L}(f, g, \tau).$$

G Additional experimental results

In this section, we present additional results to Section 4 and we follow the same setting for each dataset in Section 4.

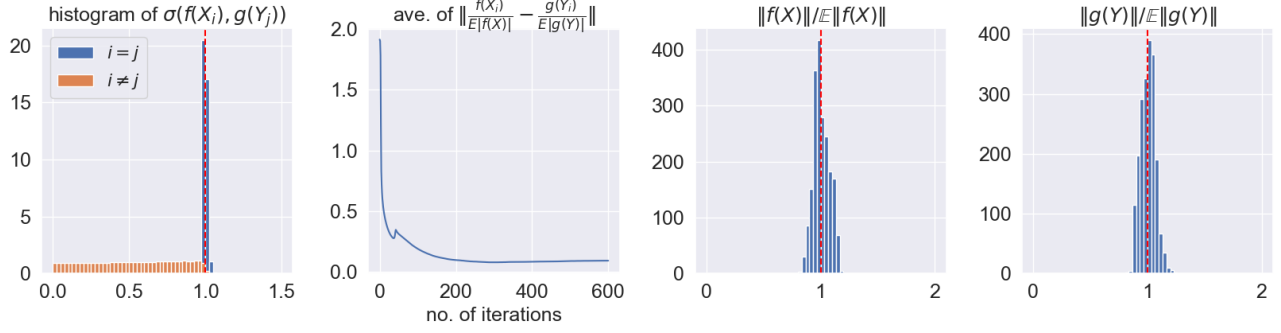


Figure 6: Histogram of similarities and norms of representations: $(d, k^*) = (3, 2)$.

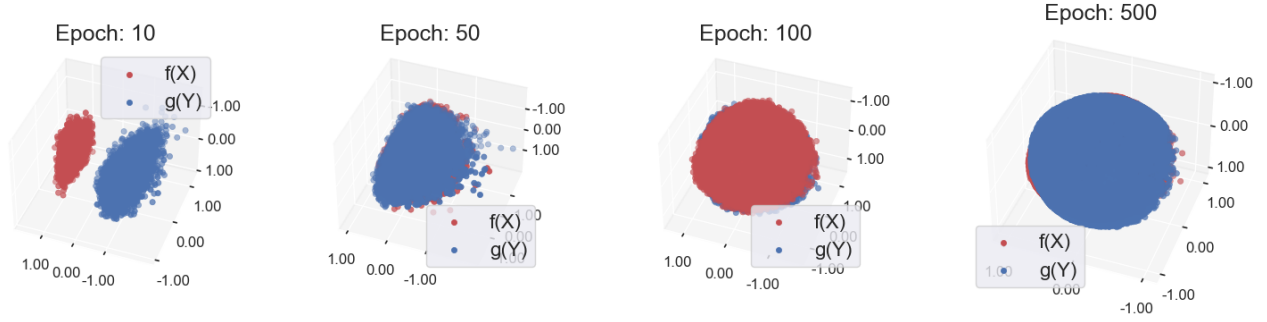


Figure 7: Scatterplots of out-of-sample representations: $(d, k^*) = (3, 2)$.

G.1 Norm concentration

Following the discussion in Section 1.1, we consider the same setting with $(d, k^*) = (3, 2)$ (Figure 6) and $(d, k^*) = (20, 5)$ (Figure 8), respectively. In addition, for the setting with $d = 3$, we also present the scatterplot for out-of-sample representations along the training process in Figure 7.

From Figure 6 and Figure 8, it is clear that $m_\sigma(f, g) = 1$ and $\|f(X)\|/\mathbb{E}\|f(X)\|, \|g(Y)\|/\mathbb{E}\|g(Y)\| \approx 1$, which indicates that $(f, g) \in \mathcal{A}(\mathcal{H})$. This empirical finding is nontrivial in the sense that in our training, there is no constraint on $\|f(X)\|/\mathbb{E}\|f(X)\|$ and $\|g(Y)\|/\mathbb{E}\|g(Y)\|$, but, when the function class \mathcal{H} is sufficiently expressive, the representations after population-level normalization tend to concentrate on the unit hypersphere automatically.

G.2 Example with $\mathcal{V}(\mathcal{H}) = \emptyset$: alignment versus simply similarity maximization

To illustrate why the assumption $\mathcal{V}(\mathcal{H}) \neq \emptyset$ is important, in this section, we use empirical examples to show that CLIP minimizers may not be semantically meaningful if $\mathcal{V}(\mathcal{H}) = \emptyset$. We consider the same setting in Section 1.1 but instead adopt the function class with 2-layer ReLU neural networks with the width of the middle layer as 50, in which case $\mathcal{A}(\mathcal{H}) = \emptyset$. It is illustrated in Figure 9 that CLIP can lead to minimizers (f, g) with $m_\sigma(f, g) = 0$, i.e., orthogonal representations. However, even in this undesired setting, the intrinsic dimension $k^* = 2$ is correctly specified.

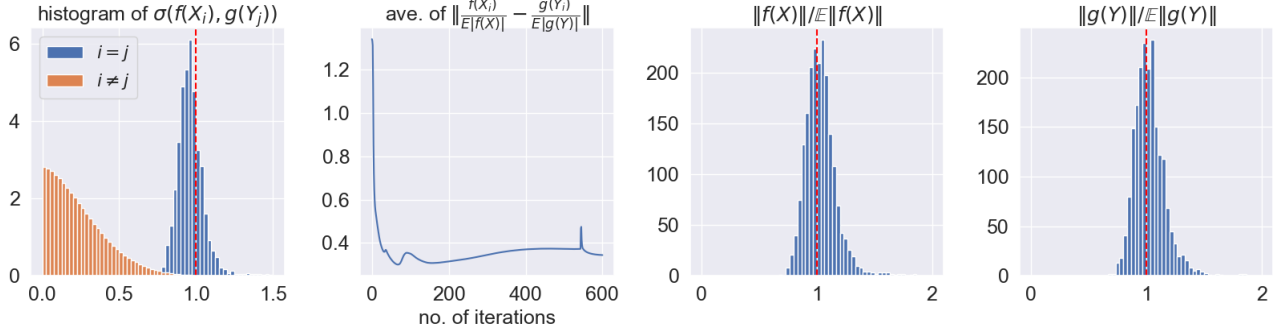


Figure 8: Histogram of similarities and norms of representations: $(d, k^*) = (20, 5)$.

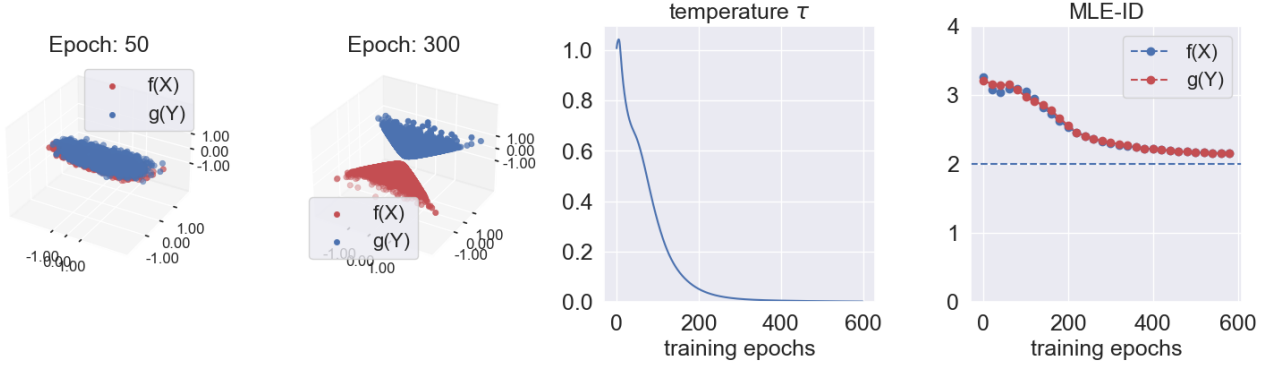


Figure 9: Results with two-layer ReLU: $m_\sigma(f, g) = 0$.

G.3 Experiment setup

We start with details of the experiment setup for real datasets. The same architecture is used in experiments: a 5-layer ReLU neural network with a width of middle-layer set to be 50 and varying input and output dimensions. The neural network is trained for 800 epochs with learning rate 10^{-4} and weight decay 10^{-4} , and a slightly faster rate is used for temperature τ : 10^{-3} in synthetic experiments and 2×10^{-4} for real data.

CITE-seq dataset. We follow the preprocessing in https://satijalab.org/seurat/articles/weighted_nearest_neighbor_analysis, where we normalize ADT data with centering to produce a 24-dimension input, and normalize the extremely high-dimensional RNA data and extract the first 200 principal components as the inputs for CLIP.

For the downstream classification tasks, we consider two set of labels. **CITE-seq** provides annotations of cells at two levels of granularity (Hao et al., 2021). For BMCs data, at level (1), 5 major cell populations include CD4 T cells, CD8 T cells, B cells, classical monocytes (CM), and natural killer (NK) cells. Cell populations are further divided into 27 finer subpopulations at level (2).

ImageNetV2 and YFCC dataset. For the image-text datasets, we first use pretrained image and text encoders to transform images and texts to numerical inputs. Concretely, we adopt a pretrained

ViT-14L from `openai/clip-vit-large-patch14`⁷ (without projection) as the image encoder and a masked self-attention Transformer as the text encoder from the same pretrained model. Then, with the pretrained encoders, we obtain 1024-dimensional image inputs and 768-dimensional text inputs.

G.4 Convergence of temperature

We vary the output dimension and present the convergence of temperature for the following three datasets.

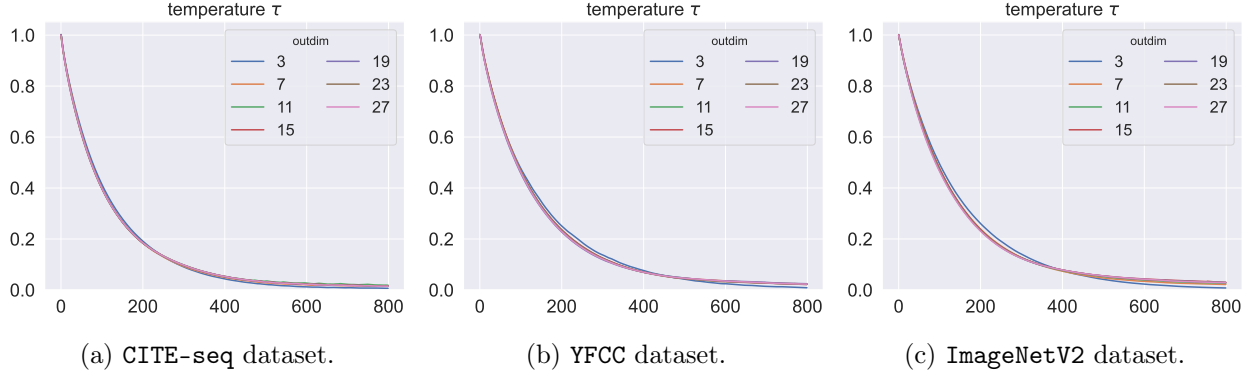


Figure 10: Convergence of temperature.

From Figure 10, we can see that with each real dataset and each choice of the output dimension, we have the temperature τ converging to zero, which is in line with our theory, and partially justifies that there are representations that can simultaneously maximize similarity and mutual information.

G.5 Comparison with cosine similarity

In this section, we present the experiment results with cosine similarity. Results for the synthetic (linear and nonlinear) and CITE-seq datasets are shown in Figure 11a, Figure 11b, and Figure 12, respectively.

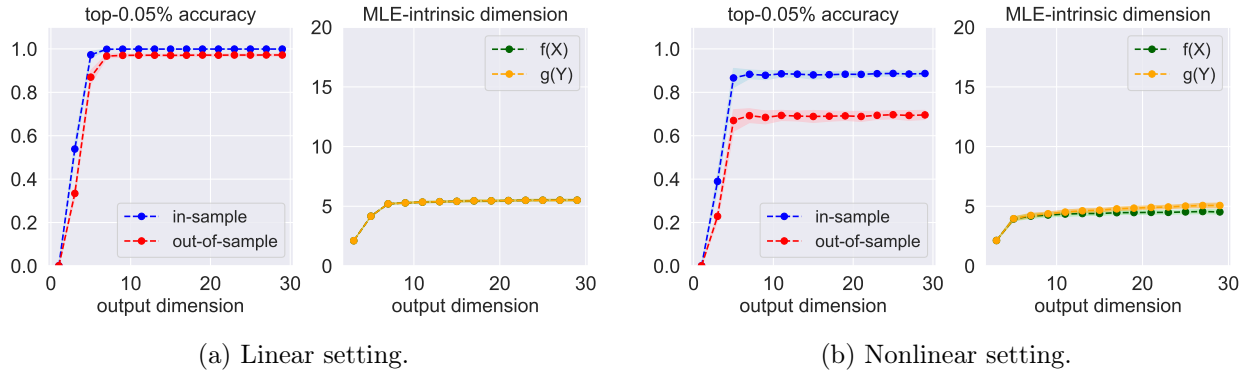


Figure 11: Results with synthetic dataset.

⁷<https://huggingface.co/openai/clip-vit-large-patch14>.

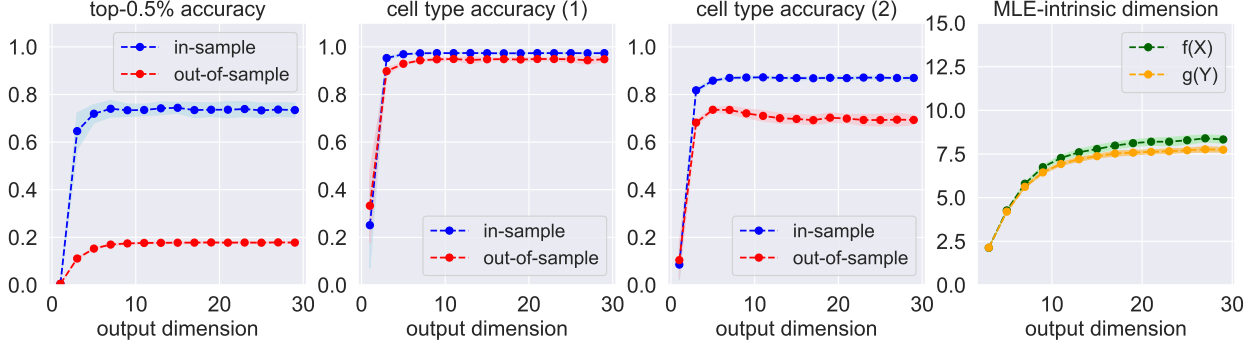


Figure 12: Results with CITE-seq dataset.

We can see that with two kinds of similarity measures, the change of estimated intrinsic dimensions with varying output dimensions is nearly the same. With the similarity measure $\sigma(\cdot, \cdot)$ adopted in the paper, the top- $\alpha\%$ accuracy is even higher for synthetic data, and in the meantime, the top- $\alpha\%$ accuracy for CITE-seq dataset is higher with cosine similarity, which is partially due to the lower signal-to-noise ratio in the dataset and cosine similarity normalizes representations more strictly. In addition, for the downstream accuracy with respect to two levels of cell types, the results with the two similarity measures are comparable.

G.6 Results with ImageNetV2 dataset

We also consider the ImageNetV2 dataset⁸ and focus on two modalities: images and text labels. Here we use the text “This is a photo of a/an **label**” as the input of the text encoder for each image. In addition, each image in ImageNetV2 dataset can be classified by coarser classes with 67 levels (Eshed, 2020), which will be adopted in a downstream classification task. We first use a pretrained image encoder (ViT-L14) and text encoder (a masked self-attention Transformer) to obtain preprocessed inputs: 1024-dimensional image embeddings and 768-dimensional text embeddings, which are used as inputs to the 5-layer ReLU neural networks. More details of preprocessing are deferred to Appendix G.

Similar to previous sections, with $|\mathcal{D}_{\text{train}}| = 8000$, $|\mathcal{D}_{\text{test}}| = 1000$, and a separate dataset with size 1000 to estimate the expected norms, we consider image classification and the top- $\alpha\%$ matching ($\alpha\% = 0.5\%$) as the downstream tasks. In addition, since images from the class share the same text input, to avoid the singularity when estimating the MLE-based intrinsic dimension, we add independent entrywise perturbations drawn from $\mathcal{N}(0, 0.01)$ to encoded text inputs before CLIP training for both $\mathcal{D}_{\text{train}}$ and $\mathcal{D}_{\text{test}}$.

We can see that both accuracies tend to saturate when d is approaching 20 and the MLE-based estimation of the intrinsic dimension for the image embeddings is approximately 8 when d keeps increasing. Since the text embeddings have a cluster structure due to discrete labels, the MLE-based intrinsic dimensions are slightly smaller than those of image embeddings. Note that we use a 5-layer ReLU network for CLIP training only for illustration purposes, and better results can potentially be obtained with more sophisticated network architectures.

⁸We load the dataset from https://github.com/modestyachts/ImageNetV2_pytorch

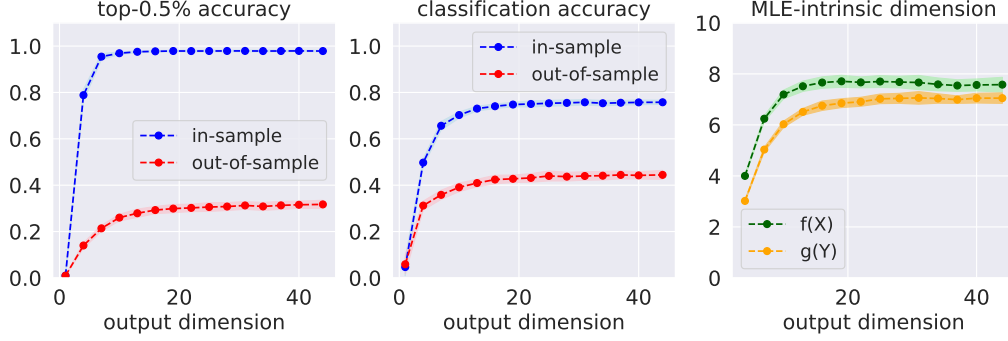


Figure 13: Results with ImageNetV2 dataset.

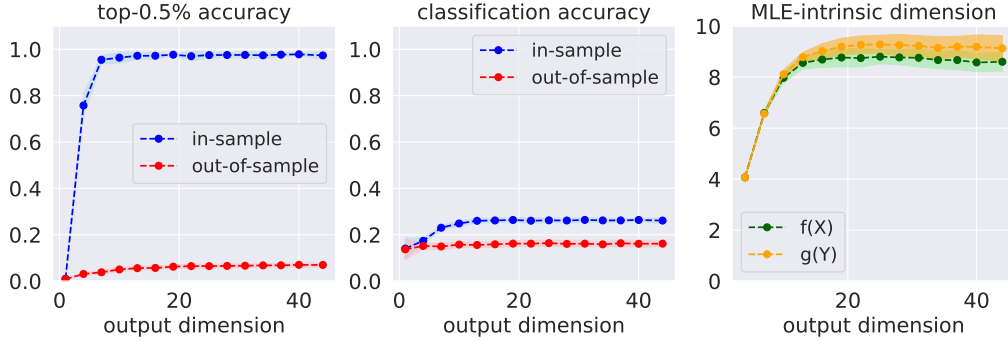


Figure 14: Results with YFCC dataset.

G.7 Results with YFCC dataset

YFCC (or YFCC100M) is a multimedia dataset consisting of images and videos as media objects with metadata including title, tags, etc (Thomee et al., 2016). We adopt a subset used by OpenAI⁹, and focus on two modalities: images and text data with descriptions of images. In addition, each image in YFCC dataset is assigned a 9-level class label (`farmid`), which will be adopted in a downstream classification task. We follow the same procedure as that in YFCC experiments. Similar to the CITE-seq experiments, we randomly sample 10000 rows without replacement from the preprocessed dataset and randomly split the subset into a training set $\mathcal{D}_{\text{train}}$ with $|\mathcal{D}_{\text{train}}| = 8000$, a test set $\mathcal{D}_{\text{test}}$ with $|\mathcal{D}_{\text{test}}| = 1000$, and a separate dataset with size 1000 to estimate the expected norms. With learned representation maps $\hat{f} \in \mathcal{F}_{\text{NN}}^{d_1, d}$, $\hat{g} \in \mathcal{F}_{\text{NN}}^{d_2, d}$, we consider image classification and the top- $\alpha\%$ matching ($\alpha\% = 0.5$) as the downstream tasks on $\mathcal{D}_{\text{test}}$. We vary the output dimension d from 1 to 29, and the results averaged after 50 repetitions are presented in Figure 14. We can see that both accuracies tend to saturate when d is around 20, and the MLE-based estimation of the intrinsic dimension for the image embeddings is approximately 9 when d keeps increasing. Similarly, we use a 5-layer ReLU network for CLIP training only for illustration purposes, and better results can potentially be obtained with more sophisticated network architectures.

⁹https://huggingface.co/datasets/dalle-mini/YFCC100M_OpenAI_subset.